processes

MDPI

Review

Successful Manufacturing Protocols of N-Rich Carbon Electrodes Ensuring High ORR Activity: A Review

Malgorzata Skorupska [1], Anna Ilnicka [1,*] and Jerzy P. Lukaszewicz [1,2]

[1] Faculty of Chemistry, Nicolaus Copernicus University in Torun, Gagarina 7, 87-100 Torun, Poland; m.skorupska@doktorant.umk.pl (M.S.); jerzy_lukaszewicz@o2.pl (J.P.L.)
[2] Centre for Modern Interdisciplinary Technologies, Nicolaus Copernicus University in Torun, Wilenska 4, 87-100 Torun, Poland
* Correspondence: ailnicka@umk.pl; Tel.: +48-609273793

Abstract: The exploration and development of different carbon nanomaterials happening over the past years have established carbon electrodes as an important electrocatalyst for oxygen reduction reaction. Metal-free catalysts are especially promising potential alternatives for replacing Pt-based catalysts. This article describes recent advances and challenges in the three main synthesis manners (i.e., pyrolysis, hydrothermal method, and chemical vapor deposition) as effective methods for the production of metal-free carbon-based catalysts. To improve the catalytic activity, heteroatom doping the structure of graphene, carbon nanotubes, porous carbons, and carbon nanofibers is important and makes them a prospective candidate for commercial applications. Special attention is paid to providing an overview on the recent major works about nitrogen-doped carbon electrodes with various concentrations and chemical environments of the heteroatom active sites. A detailed discussion and summary of catalytic properties in aqueous electrolytes is given for graphene and porous carbon-based catalysts in particular, including recent studies performed in the authors' research group. Finally, we discuss pathways and development opportunities approaching the practical use of mainly graphene-based catalysts for metal–air batteries and fuel cells.

Keywords: heteroatom doping; carbon-based nanostructure; doped graphene; oxygen reduction reaction; air electrode; metal-free electrocatalysts

check for updates

Citation: Skorupska, M.; Ilnicka, A.; Lukaszewicz, J.P. Successful Manufacturing Protocols of N-Rich Carbon Electrodes Ensuring High ORR Activity: A Review. *Processes* **2022**, *10*, 643. https://doi.org/10.3390/pr10040643

Academic Editor: Angela Scala

Received: 28 February 2022
Accepted: 17 March 2022
Published: 25 March 2022

Publisher's Note: MDPI stays neutral with regard to jurisdictional claims in published maps and institutional affiliations.

Copyright: © 2022 by the authors. Licensee MDPI, Basel, Switzerland. This article is an open access article distributed under the terms and conditions of the Creative Commons Attribution (CC BY) license (https://creativecommons.org/licenses/by/4.0/).

1. Introduction

In recent years, the technological revolution has been based predominantly on new materials with specific properties that could become alternatives to uneconomic and environmentally unfriendly materials. The search for new electrode materials can be ascribed to this trend; it is one of the key issues that need to be resolved regarding the construction of effective novel devices for energy storage and/or generation. The elimination of noble metals from electrodes is commonly seen as an essential technological problem to be solved in the upcoming years.

The oxygen reduction reaction (ORR) plays a vital role in those energy storage devices, such as fuel cells and metal–air batteries, whose high energy density makes them promising solutions [1–5]. Diverse forms of carbon materials, primarily graphene, carbon nanotubes (CNTs), amorphous carbon, and carbon nanofibers, are summarized in this paper and have been studied intensively regarding their effectiveness as electrocatalysts for ORR [6]. Carbon structures are doped with heteroatoms (e.g., boron, nitrogen, sulfur, or phosphorus) [7–10] to enhance the materials' catalytic activity. Despite extensive knowledge of the excellent activity of heteroatom-doped carbon materials in the oxygen reduction reaction, their mechanism and the function they play in ORR are still under investigation. Theoretical studies and experimental works on nitrogen-doped graphene structures consistently demonstrate promising catalytic properties that could lead such

modified materials to successfully replace platinum-based carbon catalysts. The frequently discussed substitution of carbon atoms at the edge of the graphene sheet by nitrogen gives an incomplete picture of the doping mechanism and function. Recently, experimental results have brought new insights into this topic. In the case of graphene, it has been shown that doping with nitrogen atoms causes the formation of nitrogen functional groups, not only at the edges of graphene sheets, but also built into the structure, forming pyrrolic nitrogen (N-5), pyridinic nitrogen (N-6), and graphitic nitrogen (N-Q) [11]. Thus, many problems remain to be solved [12] in the area of carbon material applicability to ORR. Due to the low catalytic activity of carbon materials in acidic solutions, further design and fabrication of new materials to be used in energy storage devices is required.

Insertion of nitrogen atoms onto the surface of graphene materials can also lead to the formation of defects, for instance, at the edges of carbon tubes and graphene planes. Another set of effects may occur upon carbonization at high temperatures, which in general increases the level of graphitization and defect dissolution. These two counter-structural effects may in parallel contribute to the change of velocity and the quantity of ORR active sites, resulting in either improvement or decay of catalytic activity in ORR. It has been proven that defects of different sorts often have significant effects on the mechanism of ORR in an alkaline medium, while an analogous effect in an acidic medium is observed less intensively [13]. It has been suggested that a higher heteroatom content level results in an increased amount of defects in the structure and contributes to improved catalytic activity [14]. Nevertheless, it is a fact that a nitrogen atom in the graphene structure couples its electron pairs together with a carbon of sp^2 hybridization in the π system. The N-6 groups located in the hexahedral carbon ring are incapable of donating an electron to the delocalized π aromatic system. Conversely, N-Q groups built into the carbon atom site in the graphene plane are capable of donating an electron to the delocalized π structure [15]. Such doping is crucial for ORR improvement, since the π electrons in the hexagonal carbon rings hardly participate in the processes comprising the whole oxygen reduction reaction. Therefore, the added electrons coming from the nitrogen atom result in a higher energy density, increasing the energy level in the highest level of the carbon molecular orbital. Following the same mechanism, heteroatom dopants that exhibit an electron deficit, such as the boron atom, seek additional electrons and thus couple their orbitals in the carbon π system. Still, the problem of the most active sites is unclear. The four-electron reduction of oxygen is attributed to N-pyridine functional groups by some, while others attribute this ability to N-Q groups or the presence of both groups in the structure [16–18]. However, what researchers agree on is the hypothesis that the nitrogen atom affects the carbon structure, thus inducing the ability to adsorb oxygen molecules from the air by breaking the double bond in the O_2 molecule [19]. While H_2O molecules are produced during oxygen reduction, it is most beneficial when the electrode is hydrophobic. This avoids flooding of the electrode, which would result in blocking newly diffused oxygen molecules. The introduction of nitrogen into the structure nullifies the hydrophobic properties due to, among other things, the fact that the pretreatment of carbonaceous materials takes place with, for example, nitric acid (HNO_3), which effectively contributes to the deterioration of the catalytic activity in ORR [20,21]. During the synthesis of doped carbon structures, coassembly of oxygen groups and heteroatom groups can occur, thereby producing a defective structure and reducing the hydrophobic properties of the final material. In addition, if the electrode is devoid of these properties, the electrolyte in which the test is being conducted itself can be impaired, reducing the wettability of the electrode material. As a result, electrodes have a short lifetime.

Electrocatalytic activity is affected not only by the amount of nitrogen functional groups, but also by the type (pyridinic, graphitic, or pyrrolic nitrogen) of groups present in the structure. Nevertheless, a correlation between the percentage nitrogen content and the final catalytic activity of the materials obtained is evident. As the level of nitrogen percentage increases, the catalytic activity in ORR also increases. However, it is argued that pyridinic nitrogen and graphitic nitrogen lead to an increased catalytic activity in

the oxygen reduction reaction that bypasses the pyrrolic-nitrogen functional group. Even at the very introduction of nitrogen into the carbon structure of sp^2, it may be found that nitrogen changes the electronic properties of the carbon atoms due to the higher electronegativity of the introduced element. This change in structure, not only electron but also geometric, increases the adsorption of oxygen molecules and makes it easier to break the bond between two oxygen atoms in an O_2 molecule. As it may turn out, it is not entirely clear which nitrogen functional groups have a direct effect on catalytic activity. There are many factors that can hinder the interpretation and cause confusing hypotheses; for example, a defective structure and graphitization of carbon materials can also favorably affect the electrochemical properties in ORR [16]. The exact role of the action of N-6 and N-Q groups was attributed by Dai et al. [22], suggesting that the higher is the amount of N-6 groups, the greater it affects the increase in the initial potential, while N-Q groups affect the limiting current density in the oxygen reduction reaction. Therefore, an increased amount of these functional groups will favorably influence the final catalytic properties and the value of electrons transferred. This point is also not clear. In the pyridine nitrogen groups, which are built into the six-membered ring at the edges of the carbon structure, alkaline media can catalyze in the disproportionation of peroxide ions produced during the oxygen reduction reaction [23]. N-6 groups, due to their position, are able to donate one electron-p to the p-system in the carbon structure layers. In contrast, N-Q bonded to three neighboring atoms has the ability, due to its similar configuration with carbon, to donate electrons to the n-system [19], as shown in Figure 1.

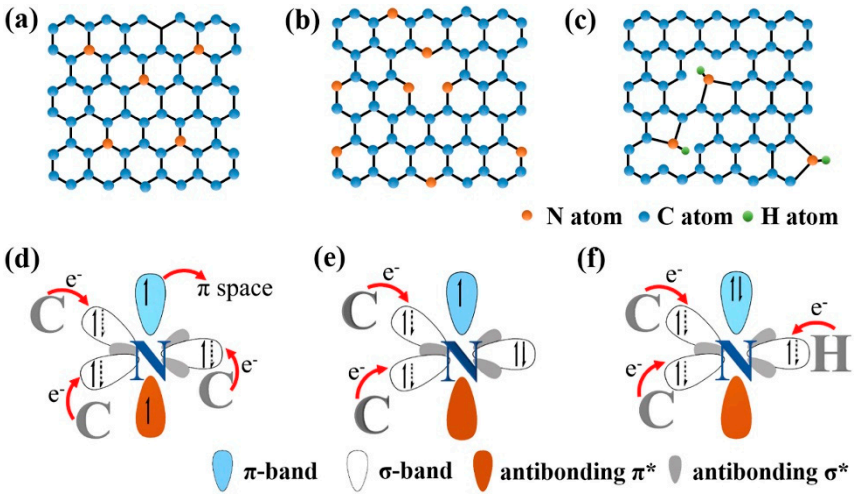


Figure 1. (**a**–**c**) Types of bonding between nitrogen and carbon configurations existing in the carbon materials: N-Q, N-6, and N-5. (**d**–**f**) A scheme of the doped atom electronic structure. Indication: * antibonding molecular orbital. Adapted from [19], with permission from *Carbon*, 2017.

The oxygen reduction reaction is a key reaction occurring at the cathode of certain energy storage devices (metal–air batteries and fuel cells), and as such is a crucial limiting factor that influences their performance [24]. It is therefore of critical importance to develop electrode materials that are highly stable and effective in ORR in both acidic and basic environments. Alkaline media is usually used, as acidic electrolytes can corrode the anodes in metal–air batteries, though this is also not without disadvantages [25]. In metal–air batteries, the charging and discharging processes are similar to those in fuel cells, and the metal ions are contained in the electrolyte. The oxygen reduction reaction occurring at the cathode can most generally be represented by several steps that occur in aqueous electrolytes: (a) oxygen molecules from the air adsorb and diffuse on the surface of the electrocatalyst; (b) electrons coming from the anode electrode are transported to the adsorbed oxygen molecules; (c) under the influence of electrons, a weakening of the bond occurs and thus the O=O bond is cleaved; (d) finally, OH^- ions that had been formed in the electrolyte are removed [25–27]. ORR can follow a more efficient one-step

pathway and exhibit a four-electron reduction of oxygen to OH^- ions (in alkaline medium, Equation (1)) or to H_2O (in acidic medium, Equation (2)), or a less efficient two-electron oxygen reduction pathway.

$$O_2 + 2H_2O + 4e^- \rightarrow 4OH^- \text{ (alkaline medium)} \quad (1)$$

$$O_2 + 4H^+ + 4e^- \rightarrow 2H_2O \text{ (acidic medium)} \quad (2)$$

For the two-electron oxygen reduction reaction, there is a two-step process with the formation of H_2O_2 intermediates, their reduction (Equations (3) and (5)), and chemical disproportionation, which increases the reaction time and requires more energy; it is necessary to minimalize this type of pathway because H_2O_2 can be aggressive while decomposing into free radicals. In both environments, the same intermediate product is present, which needs to be reduced to OH^- (Equation (4)) or to H_2O (Equation (6)), and this does not necessarily occur in one active site. In an alkaline medium, the two-electron oxygen reduction process proceeds as follows:

$$O_2 + H_2O + 2e^- \rightarrow HO_2^- + OH^- \quad (3)$$

$$HO_2^- + H_2O + 2e^- \rightarrow 3OH^- \quad (4)$$

In an acidic medium, the two-electron oxygen reduction reaction proceeds as follows:

$$O_2 + 2H^+ + 2e^- \rightarrow H_2O_2 \quad (5)$$

$$H_2O_2 + 2H^+ + 2e^- \rightarrow 2H_2O \quad (6)$$

The oxygen evolution reaction is the reverse of the oxygen reduction reaction that occurs in energy storage systems and devices. For the efficient operation of such devices, it is important that the electrode materials exhibit high stability and activity in both reactions. Slow kinetics in ORR and OER significantly reduce the performance of such devices. This problem is therefore widely researched and developed to produce catalysts that are stable in specific environments and also exhibit enhanced oxygen reduction and evolution activity for efficient reactions [28]. Researchers are looking for bifunctional catalysts that have the advantageous properties of both oxygen reduction and oxygen evolution simultaneously.

In this paper, we mainly focus on the recent achievements and critical issues affecting the field of metal-free carbon-based electrocatalysts for the oxygen reduction reaction and strategies of enhancing catalytic activity. We paid attention to nitrogen or codoped carbon nanostructures and the correlation between ORR activity and surface properties of the carbon nanomaterials. Finally, we offer personal perspectives and identify the main challenges that need to be addressed.

2. Metal-Free Cathode Electrocatalysts for Oxygen Reduction Reaction

2.1. Graphene-Based Electrocatalysts

The attention of scientists has recently been drawn to the rapid development of technology and thus the continuous demand for energy carriers, in particular electronic devices, electric vehicles, portable energy storage devices including lithium-ion batteries, fuel cells, and metal–air. Despite the existing vast knowledge and numerous publications reporting on the progress of research and development of the materials from which these devices are built, there are still various problems preventing the commercialization of many electrode materials [29,30]. The growing awareness of environmental protection demands the use of catalysts that are environmentally friendly as well as cheap and easy to recycle. In recent years, Zn–air-type batteries have gained particular interest. The Zn–air batteries that are to replace classical lead–acid and lithium-ion batteries demonstrate low production cost, high energy density, and specific capacity at low weight [31]. Researchers are continuously developing original solutions for electrode materials with high energy density, high current capacity, and safety in production and use. In order to meet these

needs, it is important to develop new methods of obtaining these materials that will successfully replace those commercially available. The current state of knowledge confirms the uniqueness of graphene and graphene-based materials. As it is known, graphene is a material with a two-dimensional (2D) structure [32]; its thickness is the size of a single atom, so it has great potential in nanotechnology. The first synthesis was based on a simple method of peeling off layers of graphite using adhesive tape to obtain a single sheet of evenly spaced carbon atoms in the shape of a honeycomb [33]. Materials based on graphene exhibit very favorable traits; even a small amount of graphene results in high mechanical and thermal stability due to its unique mechanical properties (thermal conductivity is in the range of 3000–5000 WmK^{-1}, while tensile strength is 42 Nm^{-1}) [34]. A small graphene addition affects the properties of the final product; therefore, graphene is used as a composite material or electrode material to improve its catalytic properties. The activity of pristine graphene is not high compared with commercial platinum-based electrode materials [35]. Researchers are trying to find optimal conditions for the simplest possible one-step method of obtaining heteroatom-doped graphene materials. They try to improve the electrochemical properties by modifying the structure, not only by introducing heteroatoms into the graphene structure, but by using transition metal oxides and/or transition metal molecules or polymers [36,37]. A noteworthy solution for improving the catalytic activity is the use of graphene derivatives, such as heteroatom-doped graphene quantum dots showing improved activity of electrode materials not only in ORR but also in the oxygen evolution reaction (OER) and hydrogen evolution reaction (HER) as compared with commercial electrode materials (e.g., Pt/C) [38,39]. Heteroatom-doped quantum dots are generally used to achieve a synergistic effect, which results in an increase in catalytic activity due to numerous active sites, such as defects, quasiparticles, or interfaces. The observed superb ORR performance was attributed to the charge transfer between graphene quantum dots (GQDs) and graphene nanoribbon components in tight contact, along with the numerous surface/edge defects. The heterogeneous electron transfer rate can be accelerated by increasing the density of electronic states, relating to the amount of edge defects [40]. The introduction of heteroatoms into the carbon structure causes defects in the structure that supports active sites as well as electrolyte penetration, which allows oxygen better access to the structure [41]. The structure of quantum dots resembles single- or few-layer graphene due to the precursor used in production, which is usually graphene, graphene oxide (GO), or compounds with benzene structures [42]. Heteroatom-doped graphene quantum dots can be used in combination with not only carbon material, such as graphene or carbon nanotubes, but also graphene nanowires to increase the catalytic activity of potential electrode materials [43].

This chapter specifically focuses on heteroatom-doped graphene materials and the effect types of syntheses have on the doping of carbon ORR tures, which have a significant impact on the catalytic properties in oxygen reduction reaction.

2.1.1. Synthesis of Nitrogen-Doped Graphene-Based Materials via Pyrolysis Method

An up-to-date literature review proves that graphene materials, graphene-based materials, and those with graphene-like structures are all attractive materials in terms of their properties and wide applicability. The current state of knowledge assumes that there are several ways of enriching carbon materials with nitrogen or other heteroatoms; nevertheless, nitrogen has the most positive effect on catalytic properties due to its similar atomic size and similar electronegativity [44]. There are many raw materials rich in nitrogen or other heteroatoms that, upon thermal treatment, are converted into specific functional groups or volatile compounds that enhance catalytic activity. In order for specific atoms to efficiently embed themselves into graphene structures during the carbonization process, they need a favorable correlation with carbon before thermal treatment [45]. In our recent scientific reports, we have been able to develop efficient nitrogen-doped graphene-based electrode materials [46,47]. In one of the proposed synthesis methods, we used inexpensive and environmentally friendly reagents [46], employing electroexfoliation in 1 M Na_2SO_4 to

obtain graphene sheets. Nitrogen doping of the obtained graphene structures was carried out by pyrolysis in an inert gas flow, but first, the exfoliated graphene was mixed with a nitrogen precursor, green algae (*Chlorella vulgaris*). The nitrogen content of the obtained nitrogen-doped graphene was equal to 1.8–2.2% at. However, despite this low level, the catalytic activity in the oxygen reduction reaction was comparable to the commercial Pt/C catalysis with 20% wt. of Pt. The number of transferred electrons (n) in ORR was equal to 3.78 for the sample carbonized at 800 °C. These materials were applied in practice in a Zn–air battery. In these research studies, it has been shown that even a low nitrogen content of less than 2% at. can already have a beneficial effect on the stability of the catalyst during charging–discharging of a battery. The materials obtained do not require the use of advanced recycling and are environmentally friendly as they do not contain heavy metals. In another paper by Skorupska et al. [47], metal-free graphene foams were produced using a microwave reactor and two different solvents, ethyl alcohol (EtOH) and dimethylformamide (DMF). Expanded graphite was used for the synthesis, while green algae (*Chlorella vulgaris*) were used as a natural nitrogen precursor, which incorporated N-Q and N-5 functional groups under high temperature. The calculated electron transfer number for the oxygen reduction reaction was 3.46, while for the starting material itself, without the nitrogen precursor, the value of n was 2. The methods developed so far have become an alternative way to produce completely metal-free catalysts, which have similar catalytic properties, with comparable potential for use as an electrode in metal–air batteries or fuel cells. As reported in our scientific papers, as well as written about by Qin et al. [48], ORR activity is influenced by the total content of N-6 and N-Q groups. Among other compounds, ammonium acetate [49], urea [44,50], melamine [44,51], cyanamide [44] or dicyandiamide [52,53], inorganic salts [44] such as ammonium chloride (NH_4Cl), ammonium nitrate (NH_4NO_3), ammonia gas [54], and polymers such as polypyrrole [55], polyaniline [56–58], triblock copolymers of poly (ethylene oxide)–poly(propylene oxide)–poly (ethylene oxide) [59], poly (sodium 4-styrenesulfonate), and poly (4-styrenesulfonic acid–comaleic acid) [60] are used as carriers of nitrogen functional groups converted under high-temperature processes. Quite unusual nitrogen precursors were used by Zhang et al. [61]. They designed a doped carbon material with a graphene structure using three different precursors of nitrogen, 1,3-diaminobenzene, 2,6-diaminopyridine, and 5-aminouracil (Figure 2a), to test the most beneficial nitrogen group configuration. Different configurations of these precursors produce the appropriate combination of nitrogen functional groups in the obtained materials. In this case, the most beneficial for the oxygen reduction reaction were pyridinic-N and graphitic-N functional groups with 5-aminouracil and 2,6-diaminopyridine used as precursors. These materials exhibit the highest limiting current density in linear sweep voltammetry (LSV), and the onset potential is more positive than other nitrogen groups' configurations (Figure 2b). The most advantageous configuration for N-doped graphene ($N/C\text{-}N_P + N_G$) of the four-electron oxygen reduction reaction is a combination of N-6 and N-Q groups along with N-Q predominating. However, there is no clear statement as to which acts as the most advantageous in this group. Lu et al. [62] showed that the total nitrogen content is not as important in catalytic activity as the corresponding nitrogen groups, here N-6. The use of GO and urea compounds during pyrolysis in a temperature range of 200 to 900 °C occurs at a level between 12.41% at. and 3.36% at. of nitrogen, respectively. Even small amounts of nitrogenous N-6 or N-Q functional groups, other heteroatoms, and transition metals have a beneficial influence on the catalytic properties in the oxygen reduction reaction. Increasing the nitrogen content can be achieved by using a lower carbonization temperature; however, the carbon content becomes relatively low at such temperatures [63,64].

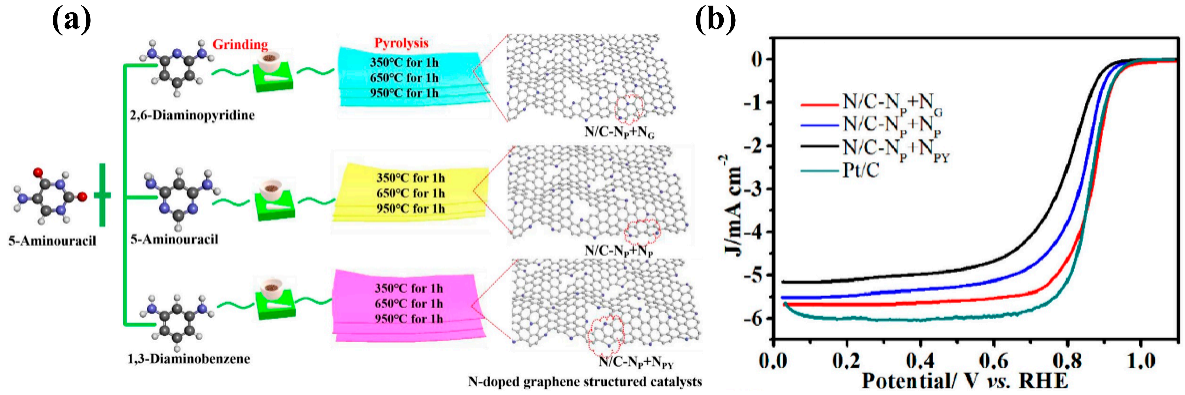


Figure 2. (**a**) Scheme of the synthesis process of precursor–modulated N–doped carbon materials; (**b**) linear scanning voltammetry curves for obtained materials. Adapted from [61], with permission from *Electrochimica Acta*, 2021.

Conversely, increasing the pyrolysis temperature increases the materials' graphitization degree from about 75% to about 85%, causing their electrical conductivity to increase [64,65]. This is the case not only for graphene materials, but generally for carbon materials of various origins. Additionally, Kabir et al. confirmed, by using the density functional theory (DFT) theoretical methods, that temperature has a significant influence on the formation of nitrogen functional groups [66,67]. They additionally put forward the hypothesis that 850 °C is the optimal temperature for the formation of an adequate amount of pyrrolic-N and pyridinic-N functional groups, with a ratio of 0.45, which increases current density in alkaline and acidic media, along with a proper correlation of the starting material and nitrogen precursor [68]. Nevertheless, an obstacle that can be encountered in the preparation of nitrogen-doped graphene materials is their structure. The pore system based on micro- and, mainly, mesopores increases oxygen access to active sites in the structure from air. As follows, surface area is important in the oxygen reduction reaction. However, in the pyrolysis process, a graphene structure has low crystallinity and tends to collapse and exhibit a low specific surface area. Therefore, the use of additional templates (silica or carbonate minerals (Na_2CO_3, $CaCO_3$)) causes an increase in the specific surface area [69,70]. Generally, the use of activators, such as KOH and NH_3 gas, is dangerous to the installation and increases the risk of damage, which in turn may cause an increase in security measures, which have a direct impact on the final production costs [63]. Table 1 summarizes the ORR activity of nitrogen-doped graphene synthesized via the pyrolysis method.

Table 1. Summary of nitrogen-doped graphene obtained via the pyrolysis method as an electrocatalyst for ORR.

Type of Sample	Precursor of Graphene	Precursor of Heteroatom(s)	S_{BET} [1] (m^2 g^{-1})	Electrolyte	Heteroatom Content	Electron Transfer Number	Ref.
N-graphene	GO [2]	PDA [3]	62.6	0.1 M KOH	n.d. [4]	3.98	[8]
N-graphene	GO	BMIM BF_4 [5]	n.d.	0.1 M KOH	4.9–7.2% at.	3.19	[11]
N-graphene	GO	Melamine	1599	0.1 M KOH	2.8% at.	2.9	[36]
N-graphene	GO	PDA	185	0.1 M KOH	3.20% at.	3.98	[37]
N-graphene	Graphite	*Chlorella vulgaris*	n.d.	0.1 M KOH	1.6–2.2% at.	3.17–3.78	[46]
N-graphene	Expanded graphite	*Chlorella vulgaris*	n.d.	0.1 M KOH	0.10–2.44% at.	2.55–3.46	[47]
N-graphene	PG [6]	NH_4 (AC)	364.5	0.1 M KOH	n.d.	3.4–4	[49]
N-graphene	GO	urea	n.d.	0.1 M KOH	7.86% at.	3.6–4	[50]
N-graphene	GO	Dicyandiamide	670	0.1 M KOH/ 0.1 M $HClO_4$	5.07% at.	>3.9	[52]
N-graphene	GO	NH_3	816	0.1 M KOH	2.4–4.6% at.	~2.75–3.25	[54]
N-graphene	GO	Urea	3.15.43	0.1 M KOH	3.46–6.65% at.	3.92	[62]
N-graphene	GO	Urea	n.d.	0.1 M KOH	8.59–20.59% at.	2.3–2	[64]

Table 1. *Cont.*

Type of Sample	Precursor of Graphene	Precursor of Heteroatom(s)	S_{BET} [1] (m^2 g^{-1})	Electrolyte	Heteroatom Content	Electron Transfer Number	Ref.
N-graphene	Graphene nanoplatelets	ADC [7]	533–657	0.1 M KOH	0.7–2.7% at.	3.04–4	[70]
N,S-graphene	GO	PDA/ 2-mercaptoethanol	273.0	0.1 M KOH	N-4.1% at. S-6.1% at.	3.52	[8]
N,S-graphene	GO	Cysteine	n.d.	0.1 M KOH	N-1.02% at. S-1.32% at.	3.47–3.72	[45]
B,N,P-graphene	GO	Boric acid/cyanamide/ phenylphosphine	443.0	0.1 M KOH/ 0.1 M $HClO_4$	N-6.45% at. B-9.98% at. P-0.6% at.	3.5	[69]

[1] S_{BET}—the specific surface area determined by the Brunauer–Emmett–Teller equation; [2] GO—graphene oxide; [3] PDA—polydopamine; [4] n.d.—not determined; [5] BMIM BF_4—1-butyl-3-methylimidazolium tetrafluoroborate; [6] PG—porous graphene; [7] ADC—azodicarbonamide.

2.1.2. Synthesis of Nitrogen-Doped Graphene-Based Materials via Hydro(Solvo)Thermal Method

Another very promising method of obtaining heteroatom-doped materials is the hydrothermal method. It is usually used in combination with pyrolysis to obtain reduced graphene oxide as a matrix for the introduction of other atoms, which would favorably influence the structure and electrochemical properties. The hydrothermal method involves introducing graphene materials such as GO or a carbon precursor, dopant atoms, and/or templates plus additives into a pressure vessel, usually made of Teflon, and then prolonged heating at about 100 to 210 °C for at least several hours, thereby creating a vacuum in the reaction vessel. A schematic of the hydro(solvo)thermal process is presented in Figure 3.

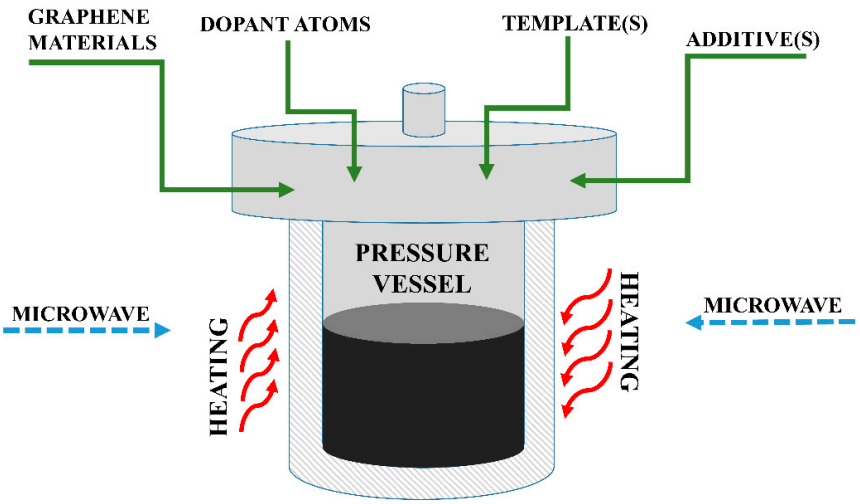


Figure 3. Schematic of stainless-steel autoclave and Teflon pressure vessel used for hydro(solvo)thermal synthesis.

In 2015, Zhou et al. [52] used synthesized graphene oxide to introduce nitrogen atoms into its structure using dicyandiamide. A hard template, silica with a particle size of about 7 nm, and $FeCl_2 \times 4\ H_2O$ were used as the separator and the reaction catalyst, respectively. They obtained graphene foam using hydrothermal treatment and stable material through pyrolysis at 900 °C in nitrogen flow for 1 h. The material was pyrolyzed twice. They demonstrated in this paper that the use of nitrogen doping and a transition metal at the same time effectively enhances the activity of the active sites, being advantageous in the oxygen reduction reaction in both alkaline and acidic media. They attribute high ORR activity to the mesoporous structure, which affects the rate of electrolithium flow, and the nitrogen functional groups (N-6 and N-Q), which are involved in the ORR reaction mechanism. Typically, researchers use a two-step synthesis of heteroatom-doped electrocatalysts: reduce

graphene oxide via a hydrothermal method using toxic reagents (e.g., hydrazine [71]), and then incorporate the heteroatoms permanently into the structure via pyrolysis [72] or apply an annealing to stabilize and introduce heteroatoms into the structure [73]. Figure 4a–f presents a scheme of the synthesis process, as well as a cross section of the structure determined by scanning electron microscopy (SEM), transmission electron microscopy (TEM), and atomic force microscopy (AFM) methods.

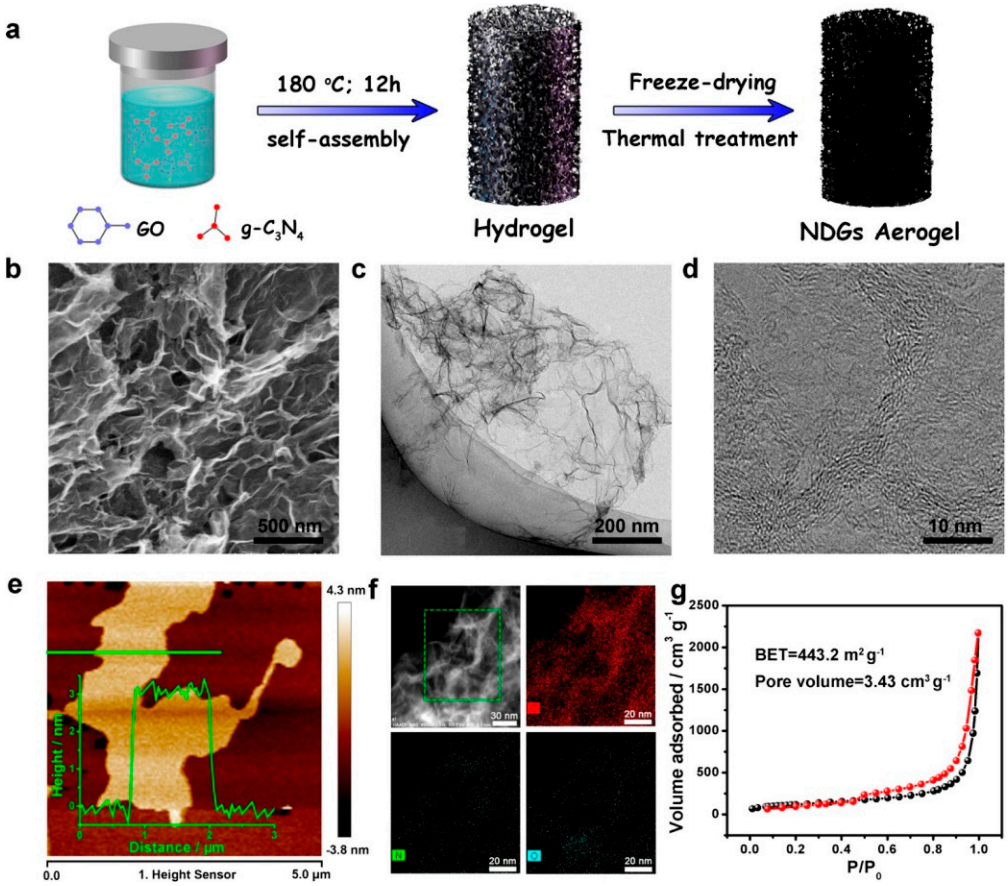


Figure 4. (**a**) Scheme of sample synthesis. (**b**) SEM, (**c**) TEM, (**d**) HRTEM, (**e**) AFM image, (**f**) elemental mapping images, and (**g**) N_2 adsorption–desorption isotherms of a representative sample. Adapted from [72], with permission from *ACS Energy Letters*, 2018.

An adsorption–desorption isotherm proving porosity is presented in Figure 4g. This approach increases the cost of production, disposal, and time taken to fabricate electrode materials. In their research work, Miao et al. [74] performed a two-step synthesis of nitrogen-doped graphene. They showed that the specific surface area calculated by the Brunauer–Emmett–Teller (BET) is not a factor for enhanced activity in ORR. The effect of doping the graphene structure with heteroatoms is a decrease in the surface area. This is due to the incorporation of other atoms in the pores and at the edges of the graphene layer, thus causing a stronger defect in the structure, which in turn may have a positive effect on ORR. Nevertheless, the higher the ratio of mesopores in the structure, the easier the transport of oxygen and electrolyte in ORR [75].

Nonmetallic elements other than nitrogen (e.g., sulfur [76], phosphorus [77,78], boron [79–81], and fluorine [79]) have also been introduced to obtain effective electrocatalysts. The role sulfur plays in the oxygen reduction reaction can be attributed to the generation of positive charge by causing a change in the electron structure of carbon atoms. The produced sulfur-doped graphene materials show high electrocatalytic activity and stability in acidic and basic environments, making them environmentally friendly. Compared with nitrogen, phosphorus has a greater ability to create defects in graphene structures, and

in a different way, than nitrogen, due to its larger atomic size. Boron, on the other hand, has a similar electron configuration ($1s^2$ $2s^2$ $2p^1$) with a difference of one valence atom relative to carbon ($1s^2$ $2s^2$ $2p^2$). The B-doped graphene structure does not observe significant changes in the graphene lattice (C–C bonds) due to the slightly longer B–C bond [82]. The most favorable choice of atoms involved in codoping is one of an element with higher electronegativity and the other with a lower electronegativity than carbon (2.55) [83]. It is possible to increase the performance of ORR by introducing doping; nevertheless, it does not beat the performance of a platinum-based catalyst. Double and triple doping of graphene with heteroatoms, such as N-S [75,84], N-B [80,83], N-P [85], B-P/BNP [86], or N-S-P [87], is more advantageous, creating a synergistic effect. This effect increases the catalytic activity of doped graphene materials to more than that of materials doped with a single type of atom. There are also reports of triple doping with heteroatoms in different configurations. Much information is provided by the work of Lin et al. [86] on doping graphene using boron and phosphorus, followed by activation through NH_3, which also increases the active sites in the graphene material. The carbon precursor in this work was GO, while the B and P precursors were boron phosphate (BPO_4). All components were subjected to a hydrothermal method. In this work, the transfer electrons for mono-, double-, and triple-doping carbon materials were compared, and it was noted that the synergistic effect between different heteroatoms, in this case B–N–P, can lead to enhanced catalytic properties in ORR. For a catalyst to exhibit a four-electron oxygen reduction reaction, it has to satisfy the premise that the more positive the cathodic potential of the ORR peak and onset potential, the higher the kinetic limiting current, which may affect the final interpretation of the ORR mechanism pathway. Zhao in 2018 [88] investigated the influence of doping order with phosphorus atoms first and nitrogen atoms second on the final content and type of nitrogen functional groups (schematic of synthesis, Figure 5a). They proved experimentally and theoretically that this approach can significantly improve the catalytic activity of N-doped carbon materials. The bonding of carbon with phosphorus can occur outside the structure (externally) or be incorporated into the carbon structure (internally) (Figure 5b). Due to C–P bonding in the external system, it is possible to decrease the energy needed for the formation of C–N bond (graphite N), causing the content of N-Q functional groups to increase. The situation is quite interesting, since the mechanism of graphite-N formation at P-doped sites is theoretically presented. During nitrogen adsorption, the bond between carbon and phosphorus elongates and weakens so that graphite P can be replaced by graphite-N functional groups. Aside from codoping with heteroatoms only, codoping with nitrogen and transition metal oxides or molecules is also popular. Wu et al. [89] obtained three-dimensional (3D) structured graphene derived from nitrogen-doped graphene oxide by introducing polypyrrole and iron acetate as an iron (II, IIII) oxide (Fe_3O_4) precursor into the reaction vessel. The resulting catalyst had a higher current density in an alkaline medium, and its electron transfer exhibited a four-electron oxygen reduction pathway. Heteroatom-doped catalysts are also used as support materials for platinum or ruthenium metals, increasing their catalytic activity in oxygen reduction reactions in different environments [90]. As it is well known, the hydrothermal method is characterized by long synthesis times in order to efficiently dope with heteroatoms/transition metals or obtain the desired structural effect. Consequently, Kim et al. [91] made a successful attempt to speed up the hydrothermal synthesis by using microwaves, which effectively and quickly heat up the reaction vessel quickly [92]. Table 2 summarizes the ORR activity of nitrogen-doped graphene synthesized via the hydrothermal method.

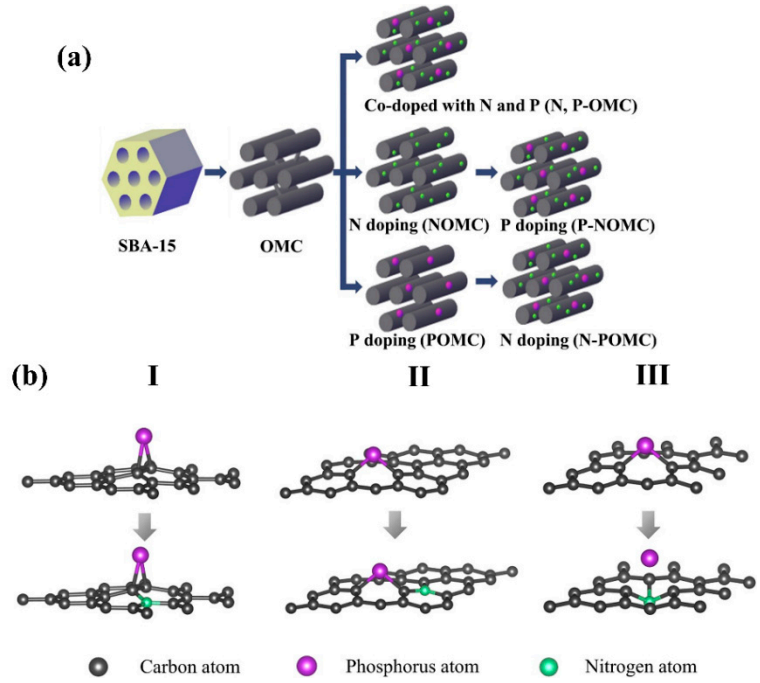


Figure 5. (**a**) Scheme of the synthesis of the N,P dual-doped OMCs; (**b**) scheme of the orientation effect of the first doped P and then doped N: (I) outside, (II) inside, (III) self-sacrifice type. Adapted from [88], with permission from the *International Journal of Hydrogen Energy*, 2018.

Table 2. Summary of nitrogen-doped graphene synthesized via the hydrothermal method as electrocatalyst for ORR.

Type of Sample	Precursor of Graphene	Precursor of Heteroatom(s)	S_{BET} (m^2 g^{-1})	Electrolyte	Heteroatom Content	Electron Transfer Number	Ref.
N-graphene	GO	Dicyandiamide	16.4–443.2	0.1 M KOH/ 0.5 M H_2SO_4	1.48–11.04% at.	~4	[72]
N-graphene	CCl_4 [1]	Pyrrole	363.7–413.6	0.1 M KOH	2.8–2.9% at.	3.88–3.81	[73]
N-graphene	GO	Urea	177.6–280.4	0.1 M KOH	3.98–6.56% at.	3.27–3.89	[74]
N-graphene	GO	Urea	489–592	0.1 M KOH	7.6–7.8% wt.	2.62–3.11	[75]
N-graphene	GO	Urea	69	0.1 M KOH	n.d. [2]	3.61	[79]
N-graphene	GO	NH_3 (gas)	n.d.	0.1 M KOH	2.8% at.	2.63	[83]
N,B-graphene	GO	NH_3/boric acid	n.d.	0.1 M KOH	N-16.57% at. B-14.37% at.	3.97	[83]
N,B-graphene	GO	$(NH_4)_2B_4O_7 \times 4H_2O$	n.d.	0.1 M KOH	N-4.25–4.43% at. B-3.03–3.55% at.	3.05–3.84	[91]
N,F-graphene	GO	Urea/TFA [3]	103	0.1 M NaOH	n.d.	3.41	[79]
N,S-graphene	GO	Urea/thiourea	374–441	0.1 M KOH	N-1.5–1.9% wt. S-1.9–2.1% wt.	3–4.05	[75]
N,S-graphene	GO	Thiourea	354.8	0.1 M KOH	N-3.13% at. S-1.31% at.	>3	[87]
N,S-graphene	GO	NH_4SCN	220	0.1 M KOH	N-4–19.7% wt. S-4.1–28.7% wt.	3.9	[84]
N,B,P-graphene	GO	NH_3/BPO_4	93–372	0.1 M KOH	N-1.98–4.50% at. B-3.73–6.53% at. P-3.07–3.80% at.	3.13–3.71	[86]
N,P,S-graphene	GO	Thiourea/TPP [4]	250.2–301.3	0.1 M KOH	N-2.88–4.34% at. S-0.89–1.24% at. P-0.96–1.31% at.	>3.4	[87]

[1] CCl_4—tetrachloromethane; [2] n.d.—not determined; [3] TFA—trifluoroacetic acid; [4] TPP—triphenylphosphine.

2.1.3. Synthesis of Nitrogen-Doped Graphene-Based Materials via Chemical Vapor Deposition Method

World literature reports that the chemical vapor deposition (CVD) method [93,94] is the one proposed so far for obtaining graphene-based electrocatalyst materials, despite

being based on uneconomical raw materials, requiring special conditions and precautions during synthesis, and using complicated apparatus. The CVD method works well in obtaining pure graphene, but is impractical on an industrial scale. Nevertheless, this method is used, which is beneficial for the content of functional groups that play a key role in the oxygen reduction reaction. The process takes place in a reaction chamber into which gaseous substrates, or heteroatom precursors, are introduced for doping in such a way that appropriate chemical reactions take place on a substrate heated to high temperatures (>800 °C). The schematic process of graphene synthesis is presented in Figure 6. Graphene is produced through different methods using high temperatures (e.g., thermal heating, plasma-enhanced CVD (PECVD) [95], or laser ablation in the presence of a catalyst (Cu, Ni)), where the carbon source and heteroatom precursors remain in close contact with hydrogen, which controls the properties of graphene. Methane (CH_4) [96,97] and ethane (C_2H_6) [93] are typically used as gaseous carbon precursors for graphene synthesis [96]. Other carbon sources can be gaseous, as well as solid or liquid [98]. Hydrocarbons decomposing to atomic sizes adsorb on the catalyst, forming specific graphene structures. One of the most popular ways to grow graphene structures of large volume and high quality is by characteristic growth on a copper sheet or foil using gaseous methane as a carbon precursor. However, this strategy for obtaining graphene is time-consuming and requires a decomposition barrier of methane (<1000 °C), the applied copper foil is not stable, and its catalytic capacity decreases as the volume of the graphene structure increases. All these factors affect energy consumption, which increases the cost of producing high-quality graphene. The homogeneity and quality of graphene, as well as the rate of the nanomaterial's formation, are negatively affected by any change in growth conditions, including the substrate/catalyst type used, synthesis temperature, pressure, carbon precursor, hydrogen or heteroatoms, and the velocity of the gas stream [99]. Doping is an effective way of properly tailoring the properties of graphene to the application of the nanomaterial in various energy storage devices. Heteroatom precursors, on the other hand, are used either simultaneously during the CVD process or in subsequent steps of heteroatom-doped graphene synthesis [100]. Nitrogen doping is usually performed using gaseous nitrogen with the simultaneous flow of carbon precursors. Commonly used carbon precursors in the CVD method includes NH_3 gas [96,97,101]. Metal-doped graphene materials possess favorable properties for the oxygen reduction reaction because of their extended structure for improved ion transportation during the redox reaction. Wu et al. [102] used the CVD method with two selected precursors, NH_3 gas and thiourea, to obtain nitrogen- and sulfur-doped graphene. As the synergetic effect improves the catalytic activity, researchers also undertake doping using analogous materials with other heteroatoms (S, B, P) and/or transition metals, all due to the growing desire to replace currently used commercial electrode materials [103]. On the other hand, Qiu et al. [94] investigated the effect of codoping with nitrogen and nickel, as well as single doping, on catalytic activity and ORR pathway determination for the potential application as metal–air batteries. They reported that Ni atoms anchored on the graphene surface and the doped nitrogen improved catalytic properties for OER and ORR reactions in an alkaline electrolyte.

The preparation of porous material using the CVD method involves chemically etching the metal substrate on which graphene structure growth occurred. While even long-lasting etching does not allow for the complete removal of metals, it can still positively influence the electrochemical properties of the obtained materials [104]. When the CVD method is used to obtain graphene, the product is a material of high quality and homogeneity, which can be beneficial for the next step of doping with graphitic C_3N_4 [14]. A combination of hard templating and the CVD method is also possible. Want et al. [105] used MgO as a template on which the graphene structure was deposited in a classical CVD method, producing a material with a specific surface area of 1440 $m^2\ g^{-1}$ and a pore volume of 2.18 $cm^3\ g^{-1}$. The result was a biofunctional catalyst for the reaction of reduction and evolution of oxygen. Shi et al. [106], using the same idea of templating by MgO, methane, and pyridine, proposed a method to obtain graphene with nitrogen dopants anchored

either in the structure or on its surface. They showed that a more advantageous concept of producing efficient electrocatalysts in ORR is to dope the graphene coating on 3D templates. This way, the final material has the morphology of the template and, after its removal, is able to expose active sites on the surface, favoring energy storage [107,108]. The final nitrogen content on the doped graphene surface was 1.81% at., and the high specific surface area was equal to 1531 m^2 g^{-1}, which together with the low defect density determined by Raman spectroscopy establishes an effective influence on the final electron transfer value in the oxygen reduction reaction, equaling 3.34. The one-step CVD synthesis method results in a uniform distribution of doped atoms in the structure with a small amount on the surface. The ORR process occurs due to the active sites having direct contact with the substrate. This means that some heteroatoms in the structure do not participate in the electron transfer process and do not contribute much to the catalytic activity of the catalyst. As established earlier, a material's atomic nitrogen content decreases as temperature increases. The CVD method makes it possible to tune the functional groups in such a way as to have them exhibit the most favorable properties for particular applications. With CVD, it is primarily possible to incorporate nitrogen in the form of N-6 and N-Q nitrogen groups. When the temperature is increased and the process is prolonged, CVD causes the amount of N-6 functional groups to decrease [109]. Previous reports indicate a limitation in the application of CVD-obtained graphene materials in acidic electrolytes due to difficulties in modifying the structure [97]. It follows that the synthesis and application of doped graphene in ORR using an acid electrolyte requires more analysis and alternative modifications to form effective electrode materials. Table 3 summarizes the ORR activity of nitrogen-doped graphene synthesized via the CVD method.

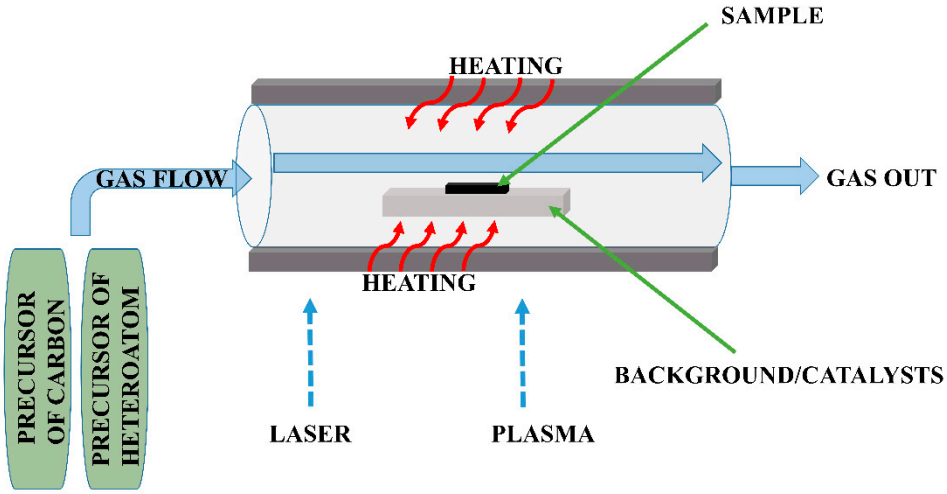


Figure 6. Schematics of synthesis chemical vapor deposition method.

Table 3. Summary of nitrogen-doped graphene synthesized via the CVD method as an electrocatalyst for ORR.

Type of Sample	Source of Carbon	Precursor of Heteroatom(s)	S_{BET} (m^2 g^{-1})	Electrolyte	Heteroatom Content	Electron Transfer Number	Ref.
N-graphene	CH_4	gC_3N_4/NH_3	830	0.1 M KOH	0.7–6.5% at.	3.86–3.88	[14]
N-graphene	CH_4	N_2 (gas)	311.7–400.2	0.1 M KOH/ 0.1 M $HClO_4$	3.8–6.7% at.	>3.9	[95]
N-graphene	CH_4	NH_3 (gas)	n.d. [1]	0.1 M $HClO_4$	n.d.	n.d.	[97]
N-graphene	CH_4	NH_3 (gas)	n.d.	0.1 M KOH	n.d.	3.6–4	[101]
N-graphene	CH_4	NH_3 (gas)	1440	0.1 M KOH	3.41% at.	>3	[105]
N-graphene	CH_4	Pyridine	1531–1732	0.1 M KOH	1.18–1.81% at.	3.34	[106]

Table 3. *Cont.*

Type of Sample	Source of Carbon	Precursor of Heteroatom(s)	S_{BET} (m^2 g^{-1})	Electrolyte	Heteroatom Content	Electron Transfer Number	Ref.
N-graphene	Pyridine	Pyridine	1000	0.1 M KOH	2.26–4.95% at.	1.1–3.9	[109]
N,S-graphene	C_2H_5OH	Thiourea	43.8–119.5	0.1 M KOH	N-4.50% at. S-0.77% at.	3.6–3.8	[102]
N,S-graphene	Pyrimidine/ thiophene	Pyrimidine/ thiophene	640	0.1 M NaOH	N-2–9.6% at. S-0.7–3.2% at.	3.2–4.1	[103]

[1] n.d.—not determined.

2.2. Carbon Nanotube-Based Electrocatalysts

As previously mentioned, despite considerable progress in nanomaterial engineering and the functionalization of materials for practical electrode applications, there is still an intense search for a cost-effective, high-performance, metal-free, and environmentally friendly method of producing materials. Many researchers focus their projects on metal-free carbon nanotubes, which have been shown to have favorable oxygen reduction properties and could become a viable alternative to commercial noble metal-based electrocatalysts. Carbon nanotubes are one of the remarkable nanomaterials that have a wide scope of potential applications in many fields, all due to their outstanding chemical stability and well-established surface functionalization techniques [110–112]. Gong et al. [113] demonstrated that nitrogen-doped carbon nanotubes possess unique properties towards an efficient oxygen reduction reaction. On that basis, an intensive search for alternative catalysts based on heteroatom-doped carbon is visible in the literature [114,115]. Many methods are known for the preparation of carbon nanotubes differing in the number of layers; this number affects the electrical and chemical properties of CNTs. As is known, among CNTs one can find single-walled carbon nanotubes (SWCNTs) consisting of one graphene layer with hexagonal packing with a diameter in the range of 0.4–2 nm and a large surface area, or multiwalled carbon nanotubes (MWCNTs) consisting of two or several layers building a cylinder wall with a diameter in the range of 1–3 nm and better conductive properties than the SWCNTs [116]. The most common methods for obtaining carbon materials in the form of cylindrical coiled graphite sheets include electric arc discharge, chemical vapor deposition, and laser ablation [110,111,117]. Carbon nanotubes have the noteworthy property of retaining atoms of other elements in a cylindrical structure. This makes CNTs attractive carbon electrode materials for fuel cells, energy storage devices, batteries, or supercapacitors. Other applications of CNTs include biosensors and devices for photocatalytic water splitting [118]. Carbon nanotubes also have applications as catalyst carriers in polymer energy fuel cells (PEFCs). Like metal-free electrocatalysts, catalysts containing transition metal oxides or base metals are also being intensively investigated [119]. During the pyrolysis of dicyandiamide, small amounts of added metal chlorides are responsible for the generation of active sites favoring the oxygen reduction reaction [120–122]. However, the main materials effective in the oxygen reduction reaction are heteroatom-doped and contain single atoms of nitrogen, sulfur, boron, phosphorus, or transition metal oxides, or are combined in double- or triple-doped carbon nanostructures. Nitrogen doping is the most widely studied. The preparation of doped carbon nanotubes can be carried out directly during their preparation, by treating previously synthesized carbon materials with heteroatom precursors [19,20]. The one-step synthesis is based on the generation of nanomaterials by pyrolysis while simultaneously embedding heteroatom precursors, while the second procedure involves a two-step synthesis, producing or obtaining previously created CNT carbon material, and then deposition/addition of heteroatoms using heteroatom precursors. One well-known strategy for obtaining efficient electrocatalysts in ORR is to combine different graphene materials exhibiting attractive end-material properties. An example is the combination of doped graphene quantum dots in carbon nanotubes (Figure 7), which is advantageous because of the apparent enhanced catalytic activity. The resulting hybrids of quantum dots and carbon nanotubes exhibit catalytic

properties owing to the heteroatom-doped dots and high conductivity owing to carbon nanotubes [123]. Carbon materials doped with transition metals also exhibit better catalytic properties in the reduction reaction or oxygen evolution reaction than expensive Pt-, Pd-, or Ir-based materials [124–127].

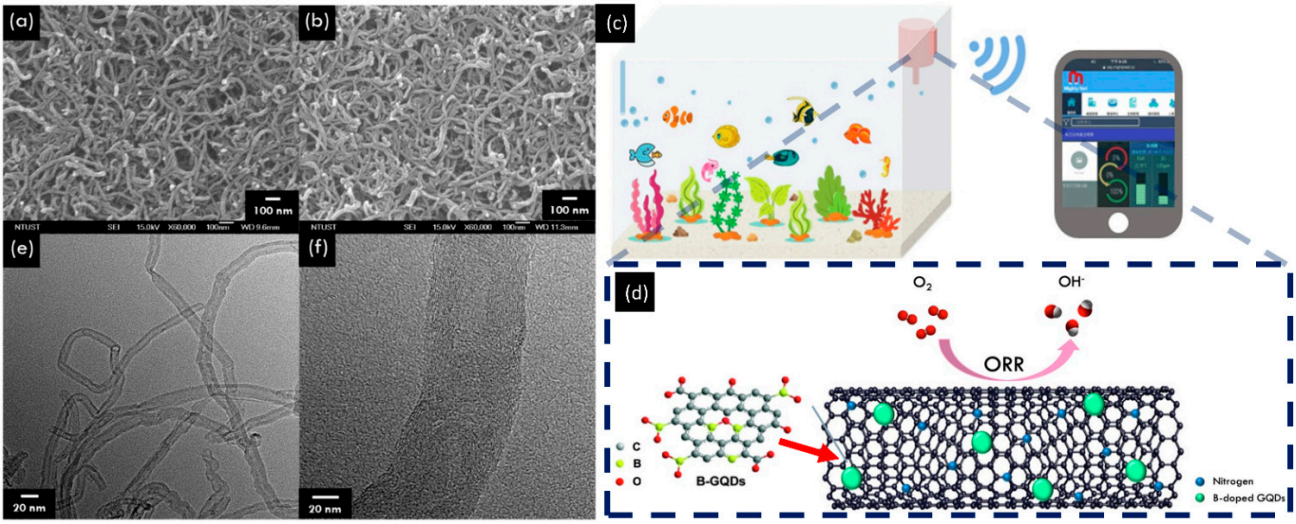


Figure 7. FE–SEM images of (**a**) CNTs, (**b**) NCNTs, (**c**) scheme of the practical application of determining dissolved oxygen, (**d**) scheme of BGQD/NCNT sample, TEM images of obtained samples in (**e**) low magnification and (**f**) high magnification. Adapted from [123], with permission from *Carbon*, 2022.

2.2.1. Synthesis of Nitrogen-Doped Carbon Nanotube-Based Materials via Pyrolysis Method

A factor contributing to the great interest in electrode materials and alternative energy source generation is the desire to reduce the cost of producing environmentally friendly, widely available carbon-based materials. To find a solution to this problem, researchers have tested various materials; the obtained electrode materials, alternative to those commercially available and typically environmentally unfriendly, are supposed to lower production costs, reduce emissions, and, above all, work effectively and have their practical application.

Nitrogen doping of carbon nanotubes is well known and has been widely studied through theoretical research, largely due to the ideal model of determining the effects of nitrogen atoms and nitrogen functional groups have in ORR [128]. Studies have also been carried out on doping with boron, sulfur, phosphorus, or silica. The researchers, after theoretical studies, came to the conclusion that nitrogen remains the atom showing superior enhanced catalytic properties in ORR. Nevertheless, Wang et al. [129] suggested a catalyst with the best achievable activity in ORR from the thermodynamic point of view that can be obtained by collating many heteroatoms in the structure, causing a synergistic effect, modifying the curvature of carbon nanotubes, and introducing characteristic defects at the ends of CNTs [130]. Gong et al. [113] were the first to demonstrate that pyrolysis-generated N-doped carbon nanotubes in the vertical position, in the presence of gaseous ammonia, exhibit enhanced catalytic activity and long-term stability in an alkaline medium, thus achieving similar performance to commercial electrodes based on platinum. The most proven method of obtaining doped carbon materials is their carbonization in the presence of a precursor for the given heteroatoms, which are directly transformed into typically volatile substances by entering into a direct reaction building into the carbon structure. The results shown by An et al. [131] demonstrate that the N-6 functional group derived from polypyrrole (nitrogen precursor) in the CNT core-shell structure plays a major role during electron transfer in the oxygen reduction reaction. The research group of Sa et al. [115] presented a synergistic effect between the CNTs' core structure and the heteroatom-doped sheath layer. The researchers demonstrated that the amount and appropriate type of

heteroatom in the sheath layer can be controlled through the correct selection of ionic liquids. This approach of creating CNT core structures that can facilitate electron transport to active sites and a cover layer doped with various heteroatoms to further enhance catalytic activity greatly contributes to improving activity in the oxygen reduction reaction. Many researchers are focused on the selection of appropriate synthesis parameters. Materials with core CNT core-shell structures can have better catalytic properties compared with double or triple heteroatom-doped carbon nanotube structures and become attractive materials for high-performance energy storage devices [115,132].

As combining the properties of two materials, in this case, carbon nanotubes and graphene, may be a good idea to improve the catalytic properties, Jiang et al. [133] investigated (a) the effect of carbonization temperature, (b) the ratio of CNTs and the precursor porous carbon structure, and (c) the effect of the ratio of carbon precursor to melamine (nitrogen precursor) on the catalytic performance of obtained materials in ORR in alkaline medium. The results show that the surface area, together with porosity, affect the catalytic activity, perhaps due to providing a large number of less active sites with better mass transfer at the same time. This is due to the amount of the nitrogen N-Q and N-6 functional groups, which affects catalytic activity in ORR. From a careful analysis, we can also find that the sample carbonized at 900 °C had more available active sites than other materials, carbonized at 800 or 1000 °C. By investigating the effect of the ratio of carbon nanotubes to glucose (as a precursor of the porous carbon sheath), the mass ratios subjected to hydrothermal treatment were examined. The lowest ratio came to 1:20, the average to 1:40, and the highest ratio to 1:80. Increasing the porous carbon precursor amount affects the final thickness of the nanoporous sheath layer. This ultimately translates into catalytic activity. A thin layer, and thus a smaller surface area, does not provide enough active sites. On the other hand, the highest ratio, 1:80, makes the shielding layer of carbon nanotubes so thick that electron transport in the oxygen reduction reaction is hindered by the low electron conductivity of the glucose-derived carbon material relative to the CNTs core. The best catalytic properties were exhibited by an average mass ratio of the reactants, 1:40. In the same work, the researchers also investigated the low, medium, and high (1:5, 1:10, 1:20) melamine content in the carbonized samples for catalytic activity in the oxygen reduction reaction. The catalyst-based electrode activity with 1:10 and 1:20 ratios showed increased initial and half-wave electrode potential. The enhanced catalytic activity was influenced by the higher amount of nitrogen precursor used; the core constructed from CNTs and a nitrogen-doped carbon nanoporous structure exhibited enhanced catalytic properties. The nanotubes formed a three-dimensional structure that was responsible for improved electron transfer, while the doped shell acted as active sites in the oxygen reduction reaction. Vikkisk et al. [23] obtained nitrogen-doped multiwalled carbon nanotubes using cyanamide or dicyandiamid. Studied catalysts showed increased selectivity towards the overall four-electron O_2 reduction pathway in alkaline media.

The use of CNTs in their hybrids or composites with graphene prevents agglomeration of graphene layers. The main problem that researchers face with graphene is that it reagglomerates very easily, which results in decreased catalytic activity, reduced specific surface area, and lower availability of active sites for the electrolyte and oxygen. To prevent this process, in many papers researchers used carbon nanotubes to counteract the reagglomeration, resulting in better accessibility for the reactants, ultimately contributing to an efficient oxygen reduction reaction. One example is a paper by Rasto et al. [15], where the authors pyrolyzed hybrids consisting of graphene oxide and multiwalled carbon nanotubes. In these studies, urea and dicyandiamide were used as nitrogen precursors, and doping was achieved by pyrolyzing the mixture of GO and MWCNTs in the presence of these nitrogen-containing compounds. Xue et al. [134] synthesized a composite of nitrogen-doped graphene nanoribbons on CNTs in an NH_3 atmosphere. The obtained materials present satisfactory high activity and stability of proton exchange membrane fuel cells. Table 4 summarizes the ORR activity of nitrogen-doped carbon nanotubes synthesized via the pyrolysis method.

Table 4. Summary of nitrogen-doped carbon nanotubes synthesized via the pyrolysis as an electrocatalyst for ORR.

Type of Sample	Type of Carbon	Precursor of Heteroatom(s)	S_{BET} (m^2 g^{-1})	Electrolyte	Heteroatom Content	Electron Transfer Number	Ref.
N-CNT	CNT	urea/DCDA [1]	n.d.	0.1 M KOH	4–6% at.	>3.5	[15]
N-CNT	CNT	melamine	104.7	0.1 M KOH	0.193% at.	2.77–2.80	[51]
N-CNT	CNT	NH_3/aniline	n.d.	0.1 M KOH	n.d.	2.5–4	[20]
N-CNT	FePc [2]	$NH_{3\ (gas)}$	n.d.	0.1 M KOH	3.6–5.6% at.	1.8–3.9	[113]
N-CNT	CNT	urea	230–284	0.1 M KOH	0.5–1.7% at.	2.9–3.55	[114]
N-CNT	CNT	urea/NH_3	n.d.	0.1 M KOH	n.d.	>3.7	[115]
N-CNT	CNT/GO	PEI [3]/DCDA	n.d.	1 M $HClO_4$	1.5–3.1% at.	3.58–3.94	[120]
N-CNT	C_2H_4	pyrrole	149.46–192.47	0.1 M KOH	5.69–6.90% at.	3.03–3.94	[131]
N-CNT	CNT	melamine	101–479	0.1 M KOH	3.54–15.76% at.	~4	[133]
N-CNT	CNT	CM [4]/DCDA	n.d.	0.1 M KOH	2.3–3.7% at.	4	[23]
N-CNT	CNT	$NH_{3\ (gas)}$	n.d.	0.1 M KOH/ 0.5 M H_2SO_4	3.09% at.	3.88–3.96/ 3.19–3.96	[134]
N,B-graphene	CNT/ BGQDs	$NH_{3\ (gas)}$/ Boric acid	n.d.	0.1 M KOH/0.01 M PBS/0.1 M $HClO_4$	N-0.5% wt. B-4.86% at.	3.2–3.5	[123]
N,S,F-graphene	CNT	BMITFSI [5]	293–489	0.1 M KOH	N-4.67.5% at. S-0.6%–1.1% at. F-0.7%–1.2% at.	3.4–4	[115]

[1] DCDA—dicyandiamide; [2] FePc—iron(II) phthalocyanine; [3] PEI—polyethylenimine; [4] CM—cyanamide; [5] BMITFSI—1-butyl-3-methylimidazolium bis(trifluoromethylsulfonyl)imide.

2.2.2. Synthesis of Nitrogen-Doped Carbon Nanotube-Based Materials via Hydrothermal Method

The modification and design of carbon nanotubes is carried out to effectively incorporate into the structure and produce highly conductive materials [135]. Patil et al. [136] combined the hydrothermal method with pyrolysis at 750 °C. They fabricated electrode materials for reduction reactions and oxygen evolution using carbon nanotubes, but also boron nitride (BN), it being a precursor of both nitrogen and boron. The research was based on the optimization of a suitable composition using different BN weight contents. The enhanced catalytic activity is attributed to synergistic effects between nitrogen and boron, but no clear trend is observed between BN weight content and catalytic properties. A comparison was made between the annealed and the hydrothermally treated material, and it was concluded that high temperature plays an important role in enhancing the activity of the ORR reaction. The onset potential of the pyrolyzed catalyst is more positive compared with the material before carbonization. Therefore, the use of pyrolysis can significantly affect the electrocatalytic properties. However, hydrothermal treatment can not only effectively introduce nitrogen heteroatoms, but also cause an improvement in hydrophobic properties, which affect the stability of the final electrodes. Hydrothermal treatment has been proven to improve the conductivity of multiwalled carbon nanotubes and the corresponding formation of oxygen groups (Figure 8). The observed improvement of catalytic properties in OER and HER reactions mainly takes place by increasing the amount of oxygen functional groups whose ability to attract electrons is stronger; these groups include ketones and carboxyl groups. However, they are also the cause of increasing hydrophilicity [137]. This method may also reduce the number of defects, which in turn can contribute to the deterioration of ORR activity. The hydrothermal method is additionally used to purify end products in order to improve the electrocatalytic properties. Nonetheless, it is worth remembering that even trace amounts of impurities from the synthesis can have a beneficial effect on the ORR process. The hydrothermal method can act as an effective and noninvasive way to functionalize MWCNTs with HNO_3. It can effectively oxidize nanotubes, but at the same time remove the amorphous carbon present on their surface, which can be a drawback in the catalytic chemical vapor deposition process [138]. Nitric acid is often used to introduce oxygen groups and thus provide better functionality of carbon nanotubes. The preoxidation method of MWSNTs was used by Huang et al. [139]. Nitrogen

atoms were doped into functionalized carbon nanotubes through a one-step hydrothermal process by introducing oxidized MWCNTs and ethylenediamine as a nitrogen precursor. Additional support and synergistic effect were produced by the resulting nitrogen-doped GQDs. The resulting double-atom-doped hybrid exhibited catalytic properties improved over a commercial-platinum-based material by showing a four-electron oxygen reduction reaction. This study sheds new light on low-cost synthesis and modification of metal-free carbon catalysts in the oxygen reduction reaction. Chem et al. [140] presented a one-step hydrothermal process for single and dual doping of sulfur and nitrogen. The advantages of this approach are the maintenance of proper electrical conductivity, preservation of a large surface area along with adequate porosity, and preservation of a multiwalled nanotube structure. The hydrothermal method does not require drastic chemicals and synthesis conditions. Therefore, this way of producing electrode materials has a high potential for heteroatom doping of carbon structures. Another approach to producing sulfur-doped carbon nanotubes is double doping as carried out by the research group of El-Sawy et al. [141]. The first modification consisted of a hydrothermal process of oxidized carbon nanotubes together with thiourea, while the second doping was performed through sonication of the obtained product from the first step together with ethanol and benzyl disulfide, carbonized at 1000 °C at the end. The researchers showed that the hydrothermal method was insufficient to obtain the right conductivity of the carbonaceous materials, though it showed the highest sulfur and oxygen content. At the same time, double doping combined with pyrolysis shows higher activity due to numerous active sites. The approach of double doping using different methods can contribute to the development of metal-free electrocatalysts, creating a new perspective on the modification of carbon materials used in the reduction reaction of oxygen, carbon dioxide, or hydrogen evolution.

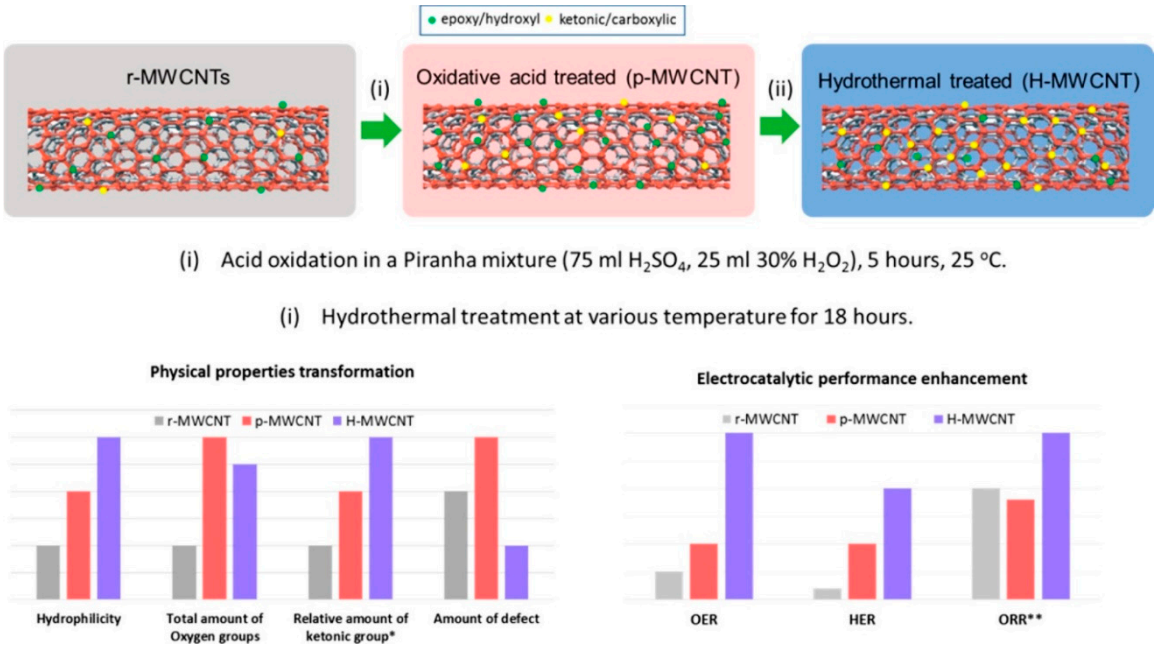


Figure 8. Graph of the effect of the hydrothermal treatment method on the change in physical properties and improvement in electrocatalytic performance (values on the graph for demonstration purposes). Indication: * ketonic group has been demonstrated to catalyze a number of electrochemically important reaction such as OER and HER, ** the ORR performance of r-MWCNT was found to be higher due to the presence of surface bound metal impurities. Adapted from [137], with permission from *ACS Applied Materials & Interfaces*, 2016.

2.2.3. Synthesis of Nitrogen-Doped Carbon Nanotube-Based Materials via Chemical Vapor Deposition Method

The CVD method is a widely studied way to produce carbon nanotubes of very high quality. As a result of the high temperature in the reaction chamber, precursors are broken down into smaller components (final product or as a layer). The precursors can be delivered with the other carbon precursors, or in the furnace, and carried by the carrier gas. Previous studies based on the synthesis of nitrogen-doped carbon nanotubes by CVD using various nitrogen–carbon precursors show less favorable catalytic properties in the oxygen reduction reaction when the medium is acidic rather than alkaline. Alexeyeva et al. [142] synthesized nitrogen-doped carbon nanotubes (with 3% at. of nitrogen) simultaneously using acetonitrile as nitrogen and carbon precursors. The researchers presented a comparison of electrochemical properties of nitrogen-doped carbon nanotubes and pure unmodified ones in the research paper. They conducted electrochemical studies on sulfuric acid and potassium hydroxide as electrolytes. Despite their best efforts, activity in ORR in an acidic medium remained lower than for the catalysts fabricated from carbon nanotubes based on platinum [143]. Wong et al. [144] investigated the effect of different nitrogen precursors on the catalytic properties in acidic medium as well. Iron (II) phthalocyanine was used as a catalyst for one-step doping and growth of carbon nanotubes using the CVD method. Three nitrogen precursors were compared, aniline, diethylamine, and ethylenediamine (EDA). At elevated temperatures, the metal catalyst is decomposed into smaller iron molecules, which form the base for nanotube growth, and the hydrocarbon catalyst, which produces a graphitic structure deposited on the iron base. The iron molecules are removed in the final process with sulfuric acid. The carbon nanotubes produced using EDA exhibited higher electrochemical activity at ORR in an acidic medium relative to the other nitrogen-rich CNTs synthesized with aniline and diethylamine. The electrochemical properties of the best test sample also stemmed from the surface structure, due to corrugation, and the extensive distribution of defects, which can act as active sites or cause better access to the edge functional groups. Other researchers, Gonzalez et al. [145], used melamine as a source of nitrogen and carbon and ferrocene as a catalyst for the growth of N-doped nanotubes to investigate the electrochemical properties in an acidic environment. As expected, the materials produced at 900 °C exhibited higher ORR activity relative to 800 °C synthesis. They concluded through Raman spectroscopy analysis and final electrochemical results that temperature affects the amount of defects generated by introducing more nitrogen heteroatoms. They also investigated the effect of the flow rate of the carrier gas, argon. In this case, they came up with a bold hypothesis that as the flow rate of argon increases, the value of the current density limiting diffusion is higher. However, there are no direct reports that this hypothesis is backed up by many experiments. It is known, however, that the rate at which a carrier gas flows influences physicochemical properties. It appears that a higher carrier gas rate results in a low number of defects, which in turn may contribute to lower activity in the ORR. Therefore, it is important to tune and optimize the synthesis conditions, carrier gas flow, and temperature and select appropriate precursors and catalysts that will benefit nitrogen incorporation into the structures that will be the active sites in ORR in an acidic environment.

The CVD method is also useful for preparing hybrids containing N-CNTs and $LaNiO_3$ [146]. In this synthesis, ammonia and methane were used to obtain the nitrogen-doped nanotubes, and acted as nitrogen and carbon precursors, respectively. Thanks to the La and Ni present in the hybrid, it is possible to support the adsorption of oxygen molecules, as well as facilitate electron transfer. The transition metals do not form direct active sites but support active sites, making them more accessible to provide higher catalytic activity [147,148]. Therefore, the use of other transition metals, such as Co, Zn, and Fe, can increase the catalytic activity, as many researchers suggest that catalytic properties stem from special metal–carbon confluence [147,149]. Not only do transition metals increase catalytic activity; hence in the case of graphene, scientists also try doping carbon nanotubes with other heteroatoms. Yang et al. [150] showed that the number of electrons transferred in the oxygen reduction

reaction increased slightly for boron-doped carbon nanotubes; the number of transferred electrons increased from 2.2 to 2.5 for undoped CNTs and boron-doped CNTs, respectively. In the case of a sample codoped with boron and nitrogen, the transfer also showed a two-electron pathway for oxygen reduction [151]. Although boron doping alone does not show spectacular catalytic activity, the instructive nature of the work is evident, because it provides much information on what to avoid when optimizing synthesis conditions. Table 5 summarizes the ORR activity of nitrogen-doped carbon nanotubes synthesized via CVD and the hydrothermal method.

Table 5. Summary of nitrogen-doped carbon nanotubes synthesized via CVD and the hydrothermal method electrocatalyst for ORR.

Type of Sample	Type of Carbon	Precursor of Heteroatom(s)	S_{BET} (m^2 g^{-1})	Electrolyte	Heteroatom Content	Electron Transfer Number	Ref.
N-CNT	CNT/CQDs	EDA [1]	n.d.	0.1 M KOH	n.d.	3.78–3.85	[139]
N-CNT	CNT	NH_4OH	388	0.1 M KOH	1.32% at.	3.7–3.8	[140]
N-CNT	Acetonitrile	Acetonitrile	n.d.	0.1 M KOH/ 0.5 M H_2SO_4	3% at.	2–3.5/2–4	[142]
N-CNT	FePc	Aniline/DEA [2]/EDA	n.d.	0.5 M H_2SO_4	4.33–6.58% at.	3–3.6	[144]
N-CNT	Pyridine	Pyridine	n.d.	0.5 M H_2SO_4	4.29–5.6% wt. 1.8–2.5% at.	n.d.	[145]
N,B-CNT	CNT	L-aspartic/ orthoboric acid	136.2	0.1 M KOH	N-1.19% at. B-0.51% at.	3.48	[135]
N,B-CNT	CNT	BN [3]	n.d.	0.1 M KOH	n.d.	3.9	[136]
N,S-CNT	CNT	$(NH_4)_2$ S	n.d.	0.1 M KOH	N-2.65% at. S-0.76% at.	n.d.	[140]

[1] EDA—ethylenediamine; [2] DEA—diethylamine; [3] BN—boron nitride.

2.3. Porous Carbon Electrocatalysts Based on Natural Precursors

In the last 10 years, a large number of studies have focused on the synthesis of biomass-derived carbons as attractive electrocatalysts [152]. As mentioned previously, the CVD method is based on the introduction of gaseous carbon precursors or heteroatoms that will be able to deposit on the substrate and form a structure in a bottom-up approach. It is not common to use the CVD method to introduce heteroatoms in a structure based on carbon materials of natural origin. Porous materials of organic origin do not require the conversion of carbon precursors to a gaseous form, and either pyrolysis or hydrothermal methods can produce materials high in nitrogen. Therefore, these two methods are presented in more detail in the following chapters in the context of nanofibers and materials of natural origin.

A particularly promising research subject is the utilization of marine- and freshwater-derived materials as carbon and nitrogen sources, for example, seaweed [153–155], shrimp shells [156,157], fish bone [158], algae [159,160], alginate [161,162], chitin, and chitosan [163–167]. For nitrogen-doped porous carbons obtained from chitin and chitosan, the influence for catalytic properties has porosity and type of functional groups [163]. The effect of additional urea treatment on the textural, chemical, and electrocatalytic properties of the obtained carbons was also presented. The highest number of O_2-reducing electrons, equal to 3.76, was recorded for the sample obtained from chitosan. The total nitrogen content of the samples obtained was in the range of 4.85% to 10.85% wt. Nitrogen was mainly present as N-5 and N-6 groups; however, N-Q and N-X groups were present as well. The share of nitrogen in the form of N-6 and N-5 groups exceeded 80% of the total nitrogen content. For the samples obtained with urea, the total nitrogen content increased to the level of 82.8–84.8% at. Additionally, the significant share of nitrogen functions of N-5 and N-6 and N-Q type increased when increasing the carbonization temperature from 700 to 800 °C. Quílez-Bermejo et al. [58] proved that as the temperature applied during the heat treatment increases, so do increase the catalytic properties in ORR. The authors attribute the enhanced catalytic activity to an increased N-Q number at the edges. The surface area can also be seen to increase with rising carbonization temperature, from which it can be concluded that the specific surface area is one of the factors favoring an increase in catalytic

activity. Increasing the surface area, which comprises a higher density and distribution of microporous structures, may contribute to increasing the effective ORR. However, previous work suggests that there are several factors that need to be achieved and developed in order for ORR to proceed in a four-electron pathway [168]. One strategy is to develop a specific surface area, and thus porosity, which will facilitate the electrolyte and ion diffusion process. The appropriate pore size guarantees permanent electrical contact and ensures long-standing four-electron oxygen reduction [169]. The bimodal distribution of pores favors the kinetics of the ORR and the diffusion of active species [170].

Gelatin is an animal derivative that contains about 16% wt. of nitrogen; therefore, it was used in many studies as a precursor in the synthesis of catalysts [160,171–174]. It is a highly economical reagent because it is a naturally abundant and sustainable resource with high solubility in polar solvents, making it a promising precursor for nitrogen-doped carbons. An example of effective synthesis are carbon samples obtained by a method of templating gelatin with colloidal silica [160]. The hierarchical gelatin-derived porous structure showed a high density of N-containing active sites (ut to 10.08% at.) and a high specific surface area (up to 880 m^2 g^{-1}). These catalysts possess a 3D mesoporous network structure that is highly favorable for rapid ORR species transport. This efficiency is promoted by the simultaneous presence of N-5 and N-Q sites, the amount of the latter being especially important in determining ORR activity. It further depends on the carbonization temperature and greatly benefits from exposed N-Q along the outer and inner carbon sheets with a high surface area. For N-doped gelatin-derived carbons, voltammograms measured in KOH O_2-saturated electrolyte exhibit a well-defined cathodic peak (Figure 9a), and the LSV curves for the produced catalysts show a similar current density to the commercial Pt/C catalyst (presented in Figure 9b). The Koutecky–Levich plots (Figure 9c) for each catalyst were obtained from LSV at various rotational speeds. The highest electron transfer number values (Figure 9d) were equal 3.85 and 3.96; these numbers confirm that catalytic activity was equal to a four-electron ORR pathway of the commercial Pt/C catalyst.

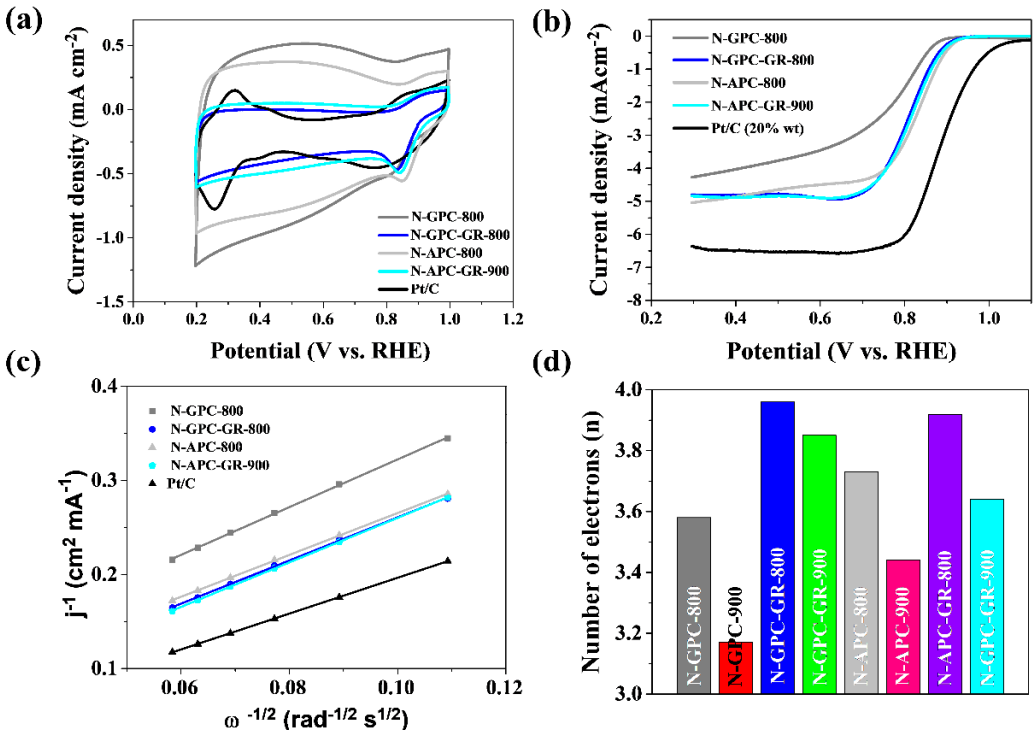


Figure 9. Results of catalyst activity in the oxygen reduction reaction for N–rich–derived carbons and the Pt/C catalyst. (**a**) CV curves of electrocatalysts in an O_2–saturated 0.1 M KOH solution, (**b**) LSV of various electrocatalysts on RDE measured at a scanning speed of 5 mV s^{-1} and a rotation speed of 1600 rpm, (**c**) Koutecky–Levich plot at 0.5 V, (**d**) number of transferred electrons. Adapted from [160], with permission from *Scientific Reports*, 2021.

In the case of nitrogen-free natural precursors such as corn stover [175], ginkgo leaves [176], coconut shell [177], or cellulose [5,178], introducing nitrogen atoms into the structure is required to obtain effective electrocatalysts for ORR. In the case of corn stover, as illustrated in Figure 10, the electrocatalyst was prepared in two major steps of KOH activation and heteroatom doping. First, corn stovers were obtained from an experiment farm and washed with water and ethanol for several times. KOH activation was a crucial element of generating a pore network in carbon this synthesis. However, the activation mechanism has not been well understood due to the large number of variables in both the experimental parameters and the reactivity of different precursors used. Summarily, the reaction starts with solid–solid (carbon and KOH) reactions. In the next step, solid–liquid reactions take place, including the reduction of potassium compounds to form metallic potassium and the oxidation of carbon to carbon oxide and carbonate [179]. For KOH carbon activation, three main activation mechanisms have been widely accepted: (I) etching the carbon framework by the redox reactions between various potassium compounds as chemical activating reagents with carbon, called chemical activation, is responsible for generating the pore network [180–182]; (II) the formation of H_2O and CO_2 in the activation system positively contributes to the further development of the porosity through the gasification of carbon, namely, physical activation; and (III) metallic potassium efficiently intercalates into the carbon lattices of the carbon matrix after its removal by washing, and the expanded carbon lattices cannot return to their previous nonporous structure, creating the high microporosity that is necessary for a large specific surface area [183].

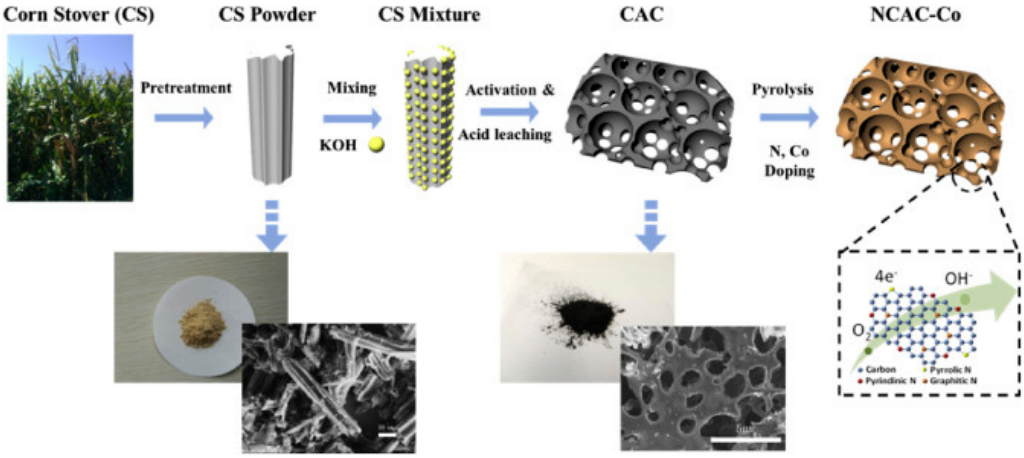


Figure 10. Schematic diagram for synthesis of N and Co, codoping NCAC-Co. Adapted from [175], with permission from *Energy*, 2018.

Depending on the nitrogen reagent used, the modification is carried out in the solid (e.g., in the case of urea), liquid (in the case of amines), or gaseous (in the case of ammonia and nitrogen oxides) [184] phase. Melamine [185], amino acids [186], acrylonitrile [187], and NH_3 gas are mainly reported as nitrogen reagents for the synthesis of nitrogen-doped porous carbon ORR catalysts. In our experience, metal-free carbon foams obtained from amino acids are valuable electrocatalysts for the four-electron oxygen reduction process [186]. A nitrogen content of up to 9.1% wt., a large surface area of up to 1287 $m^2\ g^{-1}$, and a large share of mesopores ensure full exposure of active sites, which is responsible for achieving high catalytic activity in ORR. Moreover, a high carbonization temperature of 800–900 °C ensured high electrical conductivity as a result of a more intensive graphitization process. Table 6 summarizes the ORR activity of nitrogen-doped porous carbons synthesized by pyrolysis of nitrogen-containing or nitrogen-free precursors treated by different methods.

Table 6. Summary of nitrogen-doped porous carbons derived from natural precursors as electrocatalysts for ORR.

Type of Sample	Precursor of C and N	S_{BET} (m^2 g^{-1})	Electrolyte	N Content	Electron Transfer Number	Ref.
N-C [1]	Seaweed	674.63–1217.78	0.1 M KOH	1.8–5.21% at.	3.7	[153]
N-C	Spiral seaweed	199.2–1610.3	0.1 M KOH	4.5–5.1% wt.	4	[154]
N-C	*Sargassum* spp.	3.84–188.87	0.5 M KOH	0.56–0.95% wt.	n.d. [2]	[155]
N-C	Shrimp shell	647.7	0.1 M KOH	7.44% at.	3.8	[156]
N-C	Shrimp shell	13.4–360.2	0.1 M KOH	6.8–11.8% at.	1.36–2.95	[157]
N-C	Fish bone	n.d.	0.1 M KOH	6.02% at.	n.d.	[158]
N,S-C [3]	Algae, MEL [4]	538	0.1 M KOH	2.63% at.	3.97	[159]
N-C	Green algae	366–623	0.1 M KOH	2.16–7.09% wt.	3.44–3.84	[160]
N,Co-C	Alginate	252	0.1 M KOH	2–5.5% at.	>4	[162]
N-C	Alginate	470.9	0.1 M KOH	1% at.	4	[161]
N-C	Chitin, chitosan	625–1801	0.1 M KOH	4.85–10.85% wt.	2.17–3.76	[163]
N-C	Chitosan	907	0.1 M KOH	n.d.	3.9–4	[164]
N-C	Chitosan	78–1317.97	0.1 M KOH	4.7–8.1% wt.	2.2–3.5	[165]
N-C	Chitosan	n.d.	0.1 M KOH	n.d.	3.9–4.1	[166]
N-C	Chitosan	285	0.1 M KOH	3.3–4.5% wt.	n.d.	[167]
N-C	Gelatin	376–839	0.1 M KOH	4.69–5.73% at.	3.41–4.14	[171]
N-C	Gelatin	739.5–933.9	0.1 M KOH	1.19–1.79% at.	3.7–3.85	[172]
N-C	Gelatin	189.8–1215.4	0.1 M KOH	3.6–4.3% at.	3.9–4	[173]
N-C	Gelatin	360–880	0.1 M KOH	3.24–10.08% wt.	3.17–3.85	[160]
N,Fe,Mg-C	Gelatin	370–650	0.1 M KOH	5.8–6.8% wt.	3.9–4.2	[174]
N,Co-C [6]	Corn stover, urea, $CoCl_2$	1877.3	0.1 M KOH	2.56% at.	3.87	[175]
N-C	Ginkgo leaves, NH_3	1436.02	0.1 M KOH	1.59% at.	3.7	[176]
N,P-C [5]	Coconut shells, H_3PO_4, urea	1216	0.1 M KOH	0.5–1.1% at.	4	[177]
N,P-C	Cellulose, MEL, PA [7]	241–612	0.1 M KOH	2.4–4.4% at.	3.58–3.99	[5]
N,P-C	Cellulose, $(NH_4)_3PO_4$	n.d.	PBS [8]	2.17% at.	3.5	[178]

[1] N–C—nitrogen-doped carbon; [2] n.d.—not determined; [3] N,S–C—nitrogen and sulfur-doped carbon; [4] MEL—melamine; [5] N,P–C—nitrogen and phosphorus-doped carbon; [6] N,Co–C—nitrogen and cobalt-doped carbon; [7] PA—phytic acid; [8] PBS—phosphate buffer solution.

2.4. Carbon Nanofiber-Based Electrocatalysts

Carbon nanofibers are very promising carbonaceous materials for electrochemical applications [188]. In the literature, synthesis methods such as pyrolysis [5,189,190] and chemical vapor deposition [191–194] are most widely used in large-scale production. Furthermore, electrospinning [195] is an effective carbon nanofiber synthesis method. Hydrothermal carbonization is an alternative and promising strategy of deriving a carbon nanostructure from biomass. As a carbon and nitrogen source, nitrogen-containing carbohydrates are used primarily, such as chitosan [196–199], glucosamine [200–202], and amino acids [203]. Song et al., during the hydrothermal synthesis of nitrogen-doped carbon nanofiber, used glucosamine hydrochloride and ultrathin tellurium nanowires as templates [204]. Microscopic observations indicated that the diameter of nanofibers declined from 150 to 100 nm after the pyrolysis and CO_2 activation processes (Figure 11a,b). To investigate the elemental distribution in N-CNFs-900–0.5 h, elemental mapping was undertaken using energy-filtered transmission electron microscopy (EFTEM) imaging as the analysis method (Figure 11c). The images revealed that nitrogen atoms were homogeneously distributed in the nanofibers. After heat treatment in an inert atmosphere at 900 °C and further activation with CO_2 at 1000 °C, the highly porous N-doped carbon nanofibers with a BET surface area of up to 1324.25 m^2 g^{-1} with N-5, N-6, and N-Q functional groups on the surface were produced (Figure 11d–f). The material activated with CO_2 for 4 h exhibited the optimal balance of porosity, nitrogen content, and electricity for ORR activity. The

N-CNFs-900–4 h sample displayed 3.74–4.02 transferred electrons in alkaline electrolyte at potentials ranging from −0.30 to −0.90 V.

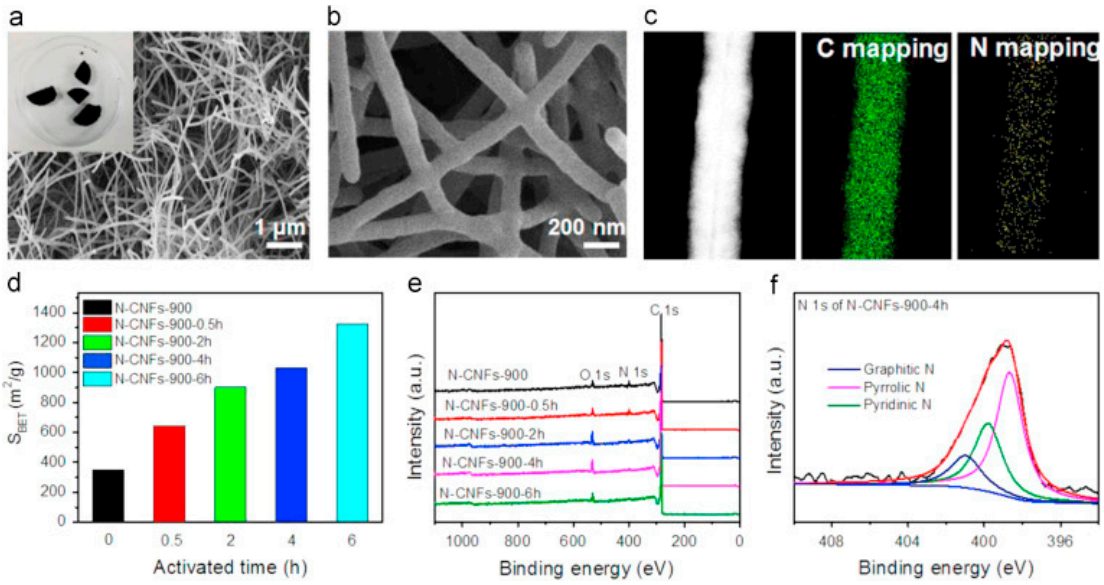


Figure 11. Characterization of the conductive and porous N-CNF aerogels obtained after pyrolysis and CO_2 activation. (**a**,**b**) SEM images at different magnifications; (**c**) EFTEM image and elemental mapping; (**d**) comparison of the BET surface areas; (**e**) XPS survey spectra; (**f**) high-resolution N1s spectra of the N-CNFs-900–4 h. Adapted from [204], with permission from *Nano Energy*, 2016.

2.4.1. Synthesis of Nitrogen-Doped Carbon Nanofiber-Based Materials via Pyrolysis Method

In the case of N-doped carbon nanofibers fabricated through carbonization, two or more precursors acting as carbon and nitrogen sources are required. By extension, the selection of proper precursors is essential to the formation of effective N-doped carbon nanofibers with high catalytic performance. Biomass is often seen as an environmentally friendly and low-cost precursor; during the last few years, bacterial cellulose in particular has attracted dramatic interest due to its production through ecofriendly microbial fermentation procedures [205]. To obtain a 3D N-CNF structure, Li et al. [206] freeze-dried bacterial-cellulose-coated polypyrrole with added $FeCl_3 \times 6\ H_2O$ before pyrolysis in a N_2 atmosphere. As a result, in the final product, higher catalytic activity was observed for N-CNFs, which possessed a higher level of pyridinic N (2.95% at.), than for pyrrolic N (1.41% at.) and graphitic N (2.02% at.). Another way to introduce nitrogen atoms to a CNF structure is their heat treatment in an NH_3 atmosphere [207]. NH_3 was also an activating agent and caused a high BET equal to 916 $m^2\ g^{-1}$. The tested N-CNF catalyst shows superior ORR activity and higher selectivity with an electron transfer number of 3.97 at 0.8 V when compared with four reference carbon materials (Vulcan XC-72R, Ketjenblack EC-300J, CNTs, and reduced graphene oxide aerogels). Excellent electrochemical stability in alkaline media for only a 20 mV negative shift of half-wave potential after 10,000 potential cycles was also determined for N-CNF aerogel [207]. Mulyadi et al. prepared carbon nanocomposites by mixing the solvothermal-treated CNFs-derived N,S-doped carbon nanofibers with complex particles of melamine–phytic acid [5]. In the next step, the suspension was allowed to sediment before lyophilization at room temperature for 4 days to form the carbon nanocomposite. Pyrolysis of the carbon nanocomposite was performed in a nitrogen atmosphere at 400 °C for 2 h, followed by another 2 h at 900 °C. The best electrocatalytic activity achieved for CNFs consisted of four heteroatoms: nitrogen (3.9% at.), sulfur (0.5% at.), phosphorus (1.9% at.), and oxygen (4.9% at.). For a good linear fitting of Koutecky–Levich plots, the desirable four-electron reduction process is predominant.

Massaglia et al. used a electrospinning technique to obtain N-CNFs from the polyacrylonitrile solution, which was then pyrolyzed at 900 °C in an inert atmosphere [189]. N-CNFs are characterized by a high amount of nitrogen groups on four states; however, the highest atomic percentage falls on graphitic N and pyridinic N, with 55.1% at. and 26.7% at., respectively. An optimal content of both N-Q and N-6 ensures a four-electron pathway towards ORR and guarantees samples' good electrical conductivity. Park et al. also used polyacrylonitrile and polystyrene in the electrospinning method [208]. For samples obtained with the pyrolysis temperature increased from 800 to 1100 °C, the onset potentials were shifted towards a more positive direction, and the limiting current density increased consecutively. For the best catalyst of N-CFs-1100 pyrolyzed at 1100 °C, the number of transferred electrons was 3.7–3.8. These results indicate that the composite samples are very promising electrocatalysts for ORR in an alkaline solution, demonstrating a highly competitive performance but at a much lower cost than the benchmarked Pt/C catalysts.

2.4.2. Synthesis of Nitrogen-Doped Carbon Nanofiber-Based Materials via Chemical Vapor Deposition Method

In the one of the pioneering papers describing the use of N-CNF in ORR, Maldonado and Stevenson prepared electrodes through a CVD method, using xylene, ferrocene, and pyridine as precursors to control nitrogen content [209]. ORR catalysts manufactured in this way showed significant activity towards the reduction of H_2O_2 in alkaline media, it being an essential stage in the whole ORR process. Some papers point out an issue related to the use of oxide catalytic supports of low electronic conductivity; that is, purification steps, such as refluxing in concentrated alkaline and acidic solutions, are necessary before employing the N-CNFs in electrocatalytic applications. An example is given in the paper by Yin et al., where post-treatment procedures with a H_2SO_4/HNO_3 mixture alter the surface chemistry and catalytic properties of the N-CNFs [210].

As reported by Bokach et al., catalytic chemical vapor deposition is an effective method for the production of nitrogen-containing carbon nanofibers in a one-step process, at a 650 °C Fe nanoparticle form, supported on expanded graphite using a mixture of CO, NH_3, and H_2 [211]. The pore formers Li_2CO_3, $(NH_4)_2CO_3$, and polystyrene microspheres were used to improve mass transport within the layer. The BET surface area and nitrogen content for the N-CNFs were 225 $m^2\ g^{-1}$ and 3.3% at., respectively. The observed large pores act as a passage for oxygen and water transport in the thick N-CNF/Fe cathodes, and thus lead to better performance. Conversely, Muthuswamy et al. [212] showed that KOH treatment resulted in similar ORR activity to pristine N-CNFs, despite growth of the surface area (BET) from 270 to 1151 $m^2\ g^{-1}$. After KOH treatment, nitrogen content drastically decreased from 4.7% at. to 0.5% at. Additionally, after activation, iron content decreased from 0.24% at. to 0.02% at.; however, the activity was much like pristine N-CNFs. The authors suggest that, besides iron or nitrogen atoms, there are active sites originating from the distinct carbon environment formed during the N-CNF synthesis. To remove iron particles from the catalyst, Buan et al. treated N-CNFs with concentrated nitric acid [192]. After HNO_3 treatment, nitrogen content was also reduced by 50% in the surface; however, ORR performance in acidic electrolyte was not affected. The authors deduced that the present porphyrin-like Fe–N_4 sites are active sites for oxygen adsorption and reduction on N-CNFs in acidic electrolyte. In a previous paper by Buan et al. [213], the influence of Fe and Ni on ORR activity was described. The oxygen reductions for N-CNF/Ni and N-CNF/Fe were two- and four-electron pathways in both acidic and alkaline electrolyte. The analyzed results may serve as an explanation of why N-doped carbon nanostructures modified by Ni show lower ORR activity when compared with those doped with Fe. However, for ORR the contribution from metallic iron, iron carbide, iron nitride, and CNFs grown from Fe can be ruled out. Table 7 summarizes the ORR activity of effective electrocatalysts based on nitrogen-doped carbon nanofibers.

Table 7. Summary of nitrogen-doped carbon nanofibers as electrocatalysts for ORR.

Type of Sample	Precursor of CNF	Precursor of Heteroatom	S_{BET} (m^2 g^{-1})	Electrolyte	N Content	Electron Transfer Number	Ref.
N-CNF	$C_6H_{13}NO_5xHCl$	$C_6H_{13}NO_5xHCl$	643–1324	0.1 M KOH	1.64–4.67% at.	3.74–4.02	[204]
N-CNF	Bacterial cellulose	C_4H_5N	215–253	0.1 M KOH/ 0.1 M $HClO_4$	4.90–8.33% at.	3.7	[206]
N-CNF	Bacterial cellulose	NH_3	916	0.1 M KOH	5.8% at.	3.96	[207]
N-CNF	PAN [1]	PAN	n.d. [2]	0.1 M KOH	2% at.	3.9	[189]
N-CNF	PAN, PS [3]	PAN	905–1271	0.1 M KOH	n.d.	3.7–3.8	[208]
N-CNF	Xylene	pyridine	130	0.5 M H_2SO_4/0.1 M KOH	4% at.	3.97	[209]
N-CNF/Fe	Graphite	NH_3	225	0.5 M H_2SO_4	3.3% at.	n.d.	[211]
N-CNF/Ni or Fe	Graphite	NH_3	35–226	0.5 M H_2SO_4/0.5 M KOH	1.5–3.9% at.	2–4	[213]
N-CNF	Graphite	NH_3	152–210	0.5 M H_2SO_4	2.4–5.1% at.	n.d.	[192]
N-CNF	Graphite	NH_3	270–1151	0.5 M H_2SO_4	0.24–4.7% at.	n.d.	[212]
N,P,S-CNF	Cellulose nanofibrils	$C_3H_6N_6$, $C_6H_{18}O_{24}P_6$	565–1217	0.5 M H_2SO_4/0.1 M KOH	2.4–4.3% wt.	3.58–3.99	[5]

[1] PAN—polyacrylonitrile; [2] n.d.—not determined; [3] PS—polystyrene.

3. Conclusions and Perspectives

In this review, we focused on nitrogen-doped, carbon-based electrodes as metal-free catalysts toward ORR. First, the mechanism of oxygen reduction in alkaline and acidic media was briefly explained. In the experimental studies, doped graphene showed the capability to catalyze oxygen reduction via a four-electron transfer pathway in alkaline electrolyte. Nevertheless, replacing a commercial Pt/C catalyst in an acidic electrolyte with doped graphene is still impossible and a challenge for research.

In experiments, a good understanding of ORR activity is possible using doped graphene quantum dots, especially with sizes closer to models used in theoretical research. Therefore, future experimental inquiries should focus more on producing graphene quantum dots and on their ORR activity in different electrolytes, as these mechanisms require additional investigation.

The methods presented in this work provide a summary of the main techniques for synthesizing nitrogen-doped carbon materials capable of being commercialized. It is not possible to say directly which synthesis technique is more efficient and promising for obtaining N-doped carbon material. Nevertheless, according to many reports, the CVD method is a good choice for obtaining multilayer carbon materials of high quality. However, one should also keep in mind the economic and ecological aspects in which the pyrolysis method fits perfectly. This method is characterized by an uncomplicated procedure for the preparation of N-doped carbon materials, as well as a significantly higher yield compared with the CVD method. On the other hand, by means of the hydrothermal method, it is possible to obtain a quantity of material that goes beyond the laboratory using safe synthesis conditions. The combination of pyrolysis and hydrothermal methods can be a perspective for obtaining materials doped with heteroatoms. Due to these advantages, methods that have large-scale commercialization potential for industrial application are presented. Small modifications of precursor amount, changes of carbon and nitrogen source, and the choice of proper temperature can contribute to obtaining materials with properties comparable to commercial ones based on heavy metals.

The influence of nitrogen sources on the final catalytic properties of the obtained carbon materials is also a very important aspect of the optimization of synthesis conditions. The selection of an appropriate precursor is a key element to successfully introducing nitrogen in the right type and amount into the carbon structure. The most commonly used nitrogen precursors include urea, melamine, and ammonia, while the most interesting

ones that fit into the concept of green chemistry are natural ones, such as chitosan, green algae, and gelatin, which all contain high amounts of nitrogen. Despite the high nitrogen content of the precursors, the final amount of introduced heteroatom is on the level of several to several tens of percent. When considering the percentage of nitrogen, the type of functional groups introduced must also be taken into account. It is still disputed among scientists attributing the direct effect of pyridine functional groups or quaternary nitrogen on catalytic activity. However, it is important to remember that both of these groups have an effect on catalytic activity. Knowing that pyridine groups are responsible for the increase of the starting potential, while quaternary nitrogen affects the limiting current density in the oxygen reduction reaction, the presence of both groups will effectively improve the final catalytic properties. It is also worth mentioning other structural and morphological properties that may help or hinder access to the active sites. A reasonable nitrogen group content maintains a high population of active sites, where the extra electrons from nitrogen correlate with π electrons in sp^2 carbon materials. Furthermore, the high performance of carbon-based electrocatalysts depends on a good balance between electron conductivity and specific surface area. However, in many papers we are unable to find information about the specific surface area, especially in the case of graphene-based electrodes; knowing that a surface area aids active sites by creating better accessibility to oxygen, an attractive prospect are those carbon foams that have an open pore system, allowing for exposed active sites and the highest possible electrolyte penetration for oxygen to reach all active sites, affecting catalytic activity.

Author Contributions: Conceptualization: A.I., M.S. and J.P.L.; writing—original draft preparation: M.S. and A.I.; writing—review and editing: A.I., M.S. and J.P.L.; supervision: A.I. and J.P.L. All authors have read and agreed to the published version of the manuscript.

Funding: This work was carried out as a result of research project no. 2019/35/N/ST5/02691, financed by the National Science Centre.

Institutional Review Board Statement: Not applicable.

Informed Consent Statement: Not applicable.

Conflicts of Interest: The authors declare no conflict of interest.

References

1. Frattini, D.; Accardo, G.; Ferone, C.; Cioffi, R. Fabrication and characterization of graphite-cement composites for microbial fuel cells applications. *Mater. Res. Bull.* **2017**, *88*, 188–199. [CrossRef]
2. Tan, P.; Chen, B.; Xu, H.; Zhang, H.; Cai, W.; Ni, M.; Liu, M.; Shao, Z. Flexible Zn-and Li-air batteries: Recent advances, challenges, and future perspectives. *Energy Environ. Sci.* **2017**, *10*, 2056–2080. [CrossRef]
3. Li, L.; Fan, W.; Xuan, J.; Leung, M.K.; Zheng, K.; She, Y. Optimal design of current collectors for microfluidic fuel cell with flow-through porous electrodes: Model and experiment. *Appl. Energy* **2017**, *206*, 413–424. [CrossRef]
4. Ren, S.; Duan, X.; Liang, S.; Zhang, M.; Zheng, H. Bifunctional electrocatalysts for Zn-air batteries: Recent developments and future perspectives. *J. Mater. Chem. A* **2020**, *8*, 6144–6182. [CrossRef]
5. Mulyadi, A.; Zhang, Z.; Dutzer, M.; Liu, W.; Deng, Y. Facile approach for synthesis of doped carbon electrocatalyst from cellulose nanofibrils toward high-performance metal-free oxygen reduction and hydrogen evolution. *Nano Energy* **2017**, *32*, 336–346. [CrossRef]
6. ElMekawy, A.; Hegab, H.M.; Losic, D.; Saint, C.P.; Pant, D. Applications of graphene in microbial fuel cells: The gap between promise and reality. *Renew. Sustain. Energy Rev.* **2017**, *72*, 1389–1403. [CrossRef]
7. Duan, J.; Chen, S.; Jaroniec, M.; Qiao, S.Z. Heteroatom-doped graphene-based materials for energy-relevant electrocatalytic processes. *ACS Catal.* **2015**, *5*, 5207–5234. [CrossRef]
8. Qu, K.; Zheng, Y.; Dai, S.; Qiao, S.Z. Graphene oxide-polydopamine derived N,S-codoped carbon nanosheets as superior bifunctional electrocatalysts for oxygen reduction and evolution. *Nano Energy* **2016**, *19*, 373–381. [CrossRef]
9. Jin, J.; Pan, F.; Jiang, L.; Fu, X.; Liang, A.; Wei, Z.; Zhang, J.; Sun, G. Catalyst-free synthesis of crumpled boron and nitrogen co-doped graphite layers with tunable bond structure for oxygen reduction reaction. *ACS Nano* **2014**, *8*, 3313–3321. [CrossRef]
10. Zhang, C.; Mahmood, N.; Yin, H.; Liu, F.; Hou, Y. Synthesis of phosphorus-doped graphene and its multifunctional applications for oxygen reduction reaction and lithium ion batteries. *Adv. Mater.* **2013**, *25*, 4932–4937. [CrossRef]
11. She, Y.; Chen, J.; Zhang, C.; Lu, Z.; Ni, M.; Sit, P.H.-L.; Leung, M.K. Nitrogen-doped graphene derived from ionic liquid as metal-free catalyst for oxygen reduction reaction and its mechanisms. *Appl. Energy* **2018**, *225*, 513–521. [CrossRef]

12. Zhang, C.; Ma, B.; Zhou, Y. Three-dimensional Polypyrrole Derived N-doped Carbon Nanotube Aerogel as a High-performance Metal-free Catalyst for Oxygen Reduction Reaction. *ChemCatChem* **2019**, *11*, 5495–5504. [CrossRef]
13. Bandosz, T.J. Porous Carbons as Oxygen Reduction Electrocatalysts. In *Porous Materials*; Springer: Berlin/Heidelberg, Germany, 2021; pp. 41–77.
14. Wu, J.; Ma, L.; Yadav, R.M.; Yang, Y.; Zhang, X.; Vajtai, R.; Lou, J.; Ajayan, P.M. Nitrogen-doped graphene with pyridinic dominance as a highly active and stable electrocatalyst for oxygen reduction. *ACS Appl. Mater. Interfaces* **2015**, *7*, 14763–14769. [CrossRef]
15. Ratso, S.; Kruusenberg, I.; Vikkisk, M.; Joost, U.; Shulga, E.; Kink, I.; Kallio, T.; Tammeveski, K. Highly active nitrogen-doped few-layer graphene/carbon nanotube composite electrocatalyst for oxygen reduction reaction in alkaline media. *Carbon* **2014**, *73*, 361–370. [CrossRef]
16. Guo, D.; Shibuya, R.; Akiba, C.; Saji, S.; Kondo, T.; Nakamura, J. Active sites of nitrogen-doped carbon materials for oxygen reduction reaction clarified using model catalysts. *Science* **2016**, *351*, 361–365. [CrossRef]
17. Liang, H.-W.; Zhuang, X.; Brüller, S.; Feng, X.; Müllen, K. Hierarchically porous carbons with optimized nitrogen doping as highly active electrocatalysts for oxygen reduction. *Nat. Commun.* **2014**, *5*, 4973. [CrossRef]
18. Ding, W.; Wei, Z.; Chen, S.; Qi, X.; Yang, T.; Hu, J.; Wang, D.; Wan, L.J.; Alvi, S.F.; Li, L. Space-confinement-induced synthesis of pyridinic-and pyrrolic-nitrogen-doped graphene for the catalysis of oxygen reduction. *Angew. Chem.* **2013**, *125*, 11971–11975. [CrossRef]
19. Deng, H.; Li, Q.; Liu, J.; Wang, F. Active sites for oxygen reduction reaction on nitrogen-doped carbon nanotubes derived from polyaniline. *Carbon* **2017**, *112*, 219–229. [CrossRef]
20. Zhao, A.; Masa, J.; Schuhmann, W.; Xia, W. Activation and stabilization of nitrogen-doped carbon nanotubes as electrocatalysts in the oxygen reduction reaction at strongly alkaline conditions. *J. Phys. Chem. C* **2013**, *117*, 24283–24291. [CrossRef]
21. Kruusenberg, I.; Ratso, S.; Vikkisk, M.; Kanninen, P.; Kallio, T.; Kannan, A.M.; Tammeveski, K. Highly active nitrogen-doped nanocarbon electrocatalysts for alkaline direct methanol fuel cell. *J. Power Source* **2015**, *281*, 94–102. [CrossRef]
22. Dai, L.; Xue, Y.; Qu, L.; Choi, H.-J.; Baek, J.-B. Metal-free catalysts for oxygen reduction reaction. *Chem. Rev.* **2015**, *115*, 4823–4892. [CrossRef]
23. Vikkisk, M.; Kruusenberg, I.; Ratso, S.; Joost, U.; Shulga, E.; Kink, I.; Rauwel, P.; Tammeveski, K. Enhanced electrocatalytic activity of nitrogen-doped multi-walled carbon nanotubes towards the oxygen reduction reaction in alkaline media. *RSC Adv.* **2015**, *5*, 59495–59505. [CrossRef]
24. Ma, R.; Ma, Y.; Dong, Y.; Lee, J.-M. Recent advances in heteroatom-doped graphene materials as efficient electrocatalysts towards the oxygen reduction reaction. *Nano Adv.* **2016**, *1*, 50–61. [CrossRef]
25. Wang, Z.-L.; Xu, D.; Xu, J.-J.; Zhang, X.-B. Oxygen electrocatalysts in metal-air batteries: From aqueous to nonaqueous electrolytes. *Chem. Soc. Rev.* **2014**, *43*, 7746–7786. [CrossRef]
26. Ma, R.; Lin, G.; Zhou, Y.; Liu, Q.; Zhang, T.; Shan, G.; Yang, M.; Wang, J. A review of oxygen reduction mechanisms for metal-free carbon-based electrocatalysts. *npj Comput. Mater.* **2019**, *5*, 78. [CrossRef]
27. Cao, R.; Lee, J.S.; Liu, M.; Cho, J. Recent progress in non-precious catalysts for metal-air batteries. *Adv. Energy Mater.* **2012**, *2*, 816–829. [CrossRef]
28. Zhao, J.; Liu, Y.; Quan, X.; Chen, S.; Zhao, H.; Yu, H. Nitrogen and sulfur co-doped graphene/carbon nanotube as metal-free electrocatalyst for oxygen evolution reaction: The enhanced performance by sulfur doping. *Electrochim. Acta* **2016**, *204*, 169–175. [CrossRef]
29. Zhu, C.; Li, H.; Fu, S.; Du, D.; Lin, Y. Highly efficient nonprecious metal catalysts towards oxygen reduction reaction based on three-dimensional porous carbon nanostructures. *Chem. Soc. Rev.* **2016**, *45*, 517–531. [CrossRef]
30. Paul, R.; Du, F.; Dai, L.; Ding, Y.; Wang, Z.L.; Wei, F.; Roy, A. 3D heteroatom-doped carbon nanomaterials as multifunctional metal-free catalysts for integrated energy devices. *Adv. Mater.* **2019**, *31*, 1805598. [CrossRef]
31. Yang, D.; Zhang, L.; Yan, X.; Yao, X. Recent progress in oxygen electrocatalysts for zinc-air batteries. *Small Methods* **2017**, *1*, 1700209. [CrossRef]
32. Cong, H.-P.; Chen, J.-F.; Yu, S.-H. Graphene-based macroscopic assemblies and architectures: An emerging material system. *Chem. Soc. Rev.* **2014**, *43*, 7295–7325. [CrossRef]
33. Novoselov, K.S.; Geim, A.K.; Morozov, S.V.; Jiang, D.-E.; Zhang, Y.; Dubonos, S.V.; Grigorieva, I.V.; Firsov, A.A. Electric field effect in atomically thin carbon films. *Science* **2004**, *306*, 666–669. [CrossRef]
34. Huang, X.; Qi, X.; Boey, F.; Zhang, H. Graphene-based composites. *Chem. Soc. Rev.* **2012**, *41*, 666–686. [CrossRef]
35. Giovanni, M.; Poh, H.L.; Ambrosi, A.; Zhao, G.; Sofer, Z.; Šaněk, F.; Khezri, B.; Webster, R.D.; Pumera, M. Noble metal (Pd, Ru, Rh, Pt, Au, Ag) doped graphene hybrids for electrocatalysis. *Nanoscale* **2012**, *4*, 5002–5008. [CrossRef]
36. Xiao, J.; Bian, X.; Liao, L.; Zhang, S.; Ji, C.; Liu, B. Nitrogen-doped mesoporous graphene as a synergistic electrocatalyst matrix for high-performance oxygen reduction reaction. *ACS Appl. Mater. Interfaces* **2014**, *6*, 17654–17660. [CrossRef]
37. Cong, H.-P.; Wang, P.; Gong, M.; Yu, S.-H. Facile synthesis of mesoporous nitrogen-doped graphene: An efficient methanol-tolerant cathodic catalyst for oxygen reduction reaction. *Nano Energy* **2014**, *3*, 55–63. [CrossRef]
38. Yan, Y.; Gong, J.; Chen, J.; Zeng, Z.; Huang, W.; Pu, K.; Liu, J.; Chen, P. Recent advances on graphene quantum dots: From chemistry and physics to applications. *Adv. Mater.* **2019**, *31*, 1808283. [CrossRef]

39. Fei, H.; Ye, R.; Ye, G.; Gong, Y.; Peng, Z.; Fan, X.; Samuel, E.L.; Ajayan, P.M.; Tour, J.M. Boron-and nitrogen-doped graphene quantum dots/graphene hybrid nanoplatelets as efficient electrocatalysts for oxygen reduction. *ACS Nano* **2014**, *8*, 10837–10843. [CrossRef]
40. Brownson, D.A.; Kampouris, D.K.; Banks, C.E. Graphene electrochemistry: Fundamental concepts through to prominent applications. *Chem. Soc. Rev.* **2012**, *41*, 6944–6976. [CrossRef]
41. Yuan, W.; Zhou, Y.; Li, Y.; Li, C.; Peng, H.; Zhang, J.; Liu, Z.; Dai, L.; Shi, G. The edge-and basal-plane-specific electrochemistry of a single-layer graphene sheet. *Sci. Rep.* **2013**, *3*, 2248. [CrossRef]
42. Tabish, T.; Zhang, S. Graphene Quantum Dots: Syntheses, Properties, and Biological Applications. In *Comprehensive Nanoscience and Nanotechnology*, 2nd ed.; Elsevier: New York, NY, USA, 2016.
43. Jin, H.; Huang, H.; He, Y.; Feng, X.; Wang, S.; Dai, L.; Wang, J. Graphene quantum dots supported by graphene nanoribbons with ultrahigh electrocatalytic performance for oxygen reduction. *J. Am. Chem. Soc.* **2015**, *137*, 7588–7591. [CrossRef] [PubMed]
44. Li, D.; Duan, X.; Sun, H.; Kang, J.; Zhang, H.; Tade, M.O.; Wang, S. Facile synthesis of nitrogen-doped graphene via low-temperature pyrolysis: The effects of precursors and annealing ambience on metal-free catalytic oxidation. *Carbon* **2017**, *115*, 649–658. [CrossRef]
45. Zhang, H.; Niu, Y.; Hu, W. Nitrogen/sulfur-doping of graphene with cysteine as a heteroatom source for oxygen reduction electrocatalysis. *J. Colloid Interface Sci.* **2017**, *505*, 32–37. [CrossRef] [PubMed]
46. Ilnicka, A.; Skorupska, M.; Romanowski, P.; Kamedulski, P.; Lukaszewicz, J.P. Improving the Performance of Zn-Air Batteries with N-Doped Electroexfoliated Graphene. *Materials* **2020**, *13*, 2115. [CrossRef]
47. Skorupska, M.; Ilnicka, A.; Lukaszewicz, J.P. N-doped graphene foam obtained by microwave-assisted exfoliation of graphite. *Sci. Rep.* **2021**, *11*, 2044. [CrossRef] [PubMed]
48. Qin, L.; Ding, R.; Wang, H.; Wu, J.; Wang, C.; Zhang, C.; Xu, Y.; Wang, L.; Lv, B. Facile synthesis of porous nitrogen-doped holey graphene as an efficient metal-free catalyst for the oxygen reduction reaction. *Nano Res.* **2017**, *10*, 305–319. [CrossRef]
49. Hassani, S.S.; Samiee, L.; Ghasemy, E.; Rashidi, A.; Ganjali, M.R.; Tasharrofi, S. Porous nitrogen-doped graphene prepared through pyrolysis of ammonium acetate as an efficient ORR nanocatalyst. *Int. J. Hydrogen Energy* **2018**, *43*, 15941–15951. [CrossRef]
50. Lin, Z.; Waller, G.; Liu, Y.; Liu, M.; Wong, C.P. Facile synthesis of nitrogen-doped graphene via pyrolysis of graphene oxide and urea, and its electrocatalytic activity toward the oxygen-reduction reaction. *Adv. Energy Mater.* **2012**, *2*, 884–888. [CrossRef]
51. Kamedulski, P.; Lukaszewicz, J.P.; Witczak, L.; Szroeder, P.; Ziolkowski, P. The Importance of Structural Factors for the Electrochemical Performance of Graphene/Carbon Nanotube/Melamine Powders towards the Catalytic Activity of Oxygen Reduction Reaction. *Materials* **2021**, *14*, 2448. [CrossRef]
52. Zhou, X.; Bai, Z.; Wu, M.; Qiao, J.; Chen, Z. 3-Dimensional porous N-doped graphene foam as a non-precious catalyst for the oxygen reduction reaction. *J. Mater. Chem. A* **2015**, *3*, 3343–3350. [CrossRef]
53. Gu, D.; Zhou, Y.; Ma, R.; Wang, F.; Liu, Q.; Wang, J. Facile synthesis of N-doped graphene-like carbon nanoflakes as efficient and stable electrocatalysts for the oxygen reduction reaction. *Nano-Micro Lett.* **2018**, *10*, 29. [CrossRef] [PubMed]
54. Yang, S.; Zhi, L.; Tang, K.; Feng, X.; Maier, J.; Müllen, K. Efficient synthesis of heteroatom (N or S)-doped graphene based on ultrathin graphene oxide-porous silica sheets for oxygen reduction reactions. *Adv. Funct. Mater.* **2012**, *22*, 3634–3640. [CrossRef]
55. Cong, K.; Radtke, M.; Stumpf, S.; Schröter, B.; McMillan, D.G.; Rettenmayr, M.; Ignaszak, A. Electrochemical stability of the polymer-derived nitrogen-doped carbon: An elusive goal? *Mater. Renew. Sustain. Energy* **2015**, *4*, 5. [CrossRef]
56. Lai, L.; Potts, J.R.; Zhan, D.; Wang, L.; Poh, C.K.; Tang, C.; Gong, H.; Shen, Z.; Lin, J.; Ruoff, R.S. Exploration of the active center structure of nitrogen-doped graphene-based catalysts for oxygen reduction reaction. *Energy Environ. Sci.* **2012**, *5*, 7936–7942. [CrossRef]
57. Wan, K.; Yu, Z.-P.; Liang, Z.-X. Polyaniline-derived ordered mesoporous carbon as an efficient electrocatalyst for oxygen reduction reaction. *Catalysts* **2015**, *5*, 1034–1045. [CrossRef]
58. Quílez-Bermejo, J.; Morallón, E.; Cazorla-Amorós, D. Oxygen-reduction catalysis of N-doped carbons prepared via heat treatment of polyaniline at over 1100 °C. *Chem. Commun.* **2018**, *54*, 4441–4444. [CrossRef]
59. Cheon, J.Y.; Kim, J.H.; Kim, J.H.; Goddeti, K.C.; Park, J.Y.; Joo, S.H. Intrinsic relationship between enhanced oxygen reduction reaction activity and nanoscale work function of doped carbons. *J. Am. Chem. Soc.* **2014**, *136*, 8875–8878. [CrossRef]
60. Florent, M.; Wallace, R.; Bandosz, T.J. Oxygen electroreduction on nanoporous carbons: Textural features vs nitrogen and boron catalytic centers. *ChemCatChem* **2019**, *11*, 851–860. [CrossRef]
61. Zhang, X.; Zhang, X.; Zhao, S.; Wang, Y.Q.; Lin, X.; Tian, Z.Q.; Shen, P.K. Precursor modulated active sites of nitrogen doped graphene-based carbon catalysts via one-step pyrolysis method for the enhanced oxygen reduction reaction. *Electrochim. Acta* **2021**, *370*, 137712. [CrossRef]
62. Lu, X.; Wang, D.; Ge, L.; Xiao, L.; Zhang, H.; Liu, L.; Zhang, J.; An, M.; Yang, P. Enriched graphitic N in nitrogen-doped graphene as a superior metal-free electrocatalyst for the oxygen reduction reaction. *New J. Chem.* **2018**, *42*, 19665–19670. [CrossRef]
63. Liu, T.; Kou, T.; Bulmahn, D.; Ortuno-Quintana, C.; Liu, G.; Lu, J.Q.; Li, Y. Tuning the electrochemical properties of nitrogen-doped carbon aerogels in a blend of ammonia and nitrogen gases. *ACS Appl. Energy Mater.* **2018**, *1*, 5043–5053. [CrossRef]
64. Xu, X.; Yuan, T.; Zhou, Y.; Li, Y.; Lu, J.; Tian, X.; Wang, D.; Wang, J. Facile synthesis of boron and nitrogen-doped graphene as efficient electrocatalyst for the oxygen reduction reaction in alkaline media. *Int. J. Hydrogen Energy* **2014**, *39*, 16043–16052. [CrossRef]

65. Huang, Z.-H.; Liu, T.-Y.; Song, Y.; Li, Y.; Liu, X.-X. Balancing the electrical double layer capacitance and pseudocapacitance of hetero-atom doped carbon. *Nanoscale* **2017**, *9*, 13119–13127. [CrossRef] [PubMed]
66. Kabir, S.; Artyushkova, K.; Serov, A.; Kiefer, B.; Atanassov, P. Binding energy shifts for nitrogen-containing graphene-based electrocatalysts-experiments and DFT calculations. *Surf. Interface Anal.* **2016**, *48*, 293–300. [CrossRef]
67. Kabir, S.; Artyushkova, K.; Kiefer, B.; Atanassov, P. Computational and experimental evidence for a new TM-N_3/C moiety family in non-PGM electrocatalysts. *Phys. Chem. Chem. Phys.* **2015**, *17*, 17785–17789. [CrossRef]
68. Kabir, S.; Artyushkova, K.; Serov, A.; Atanassov, P. Role of nitrogen moieties in N-doped 3D-graphene nanosheets for oxygen electroreduction in acidic and alkaline media. *ACS Appl. Mater. Interfaces* **2018**, *10*, 11623–11632. [CrossRef]
69. Dong, F.; Cai, Y.; Liu, C.; Liu, J.; Qiao, J. Heteroatom (B, N and P) doped porous graphene foams for efficient oxygen reduction reaction electrocatalysis. *Int. J. Hydrogen Energy* **2018**, *43*, 12661–12670. [CrossRef]
70. Skorupska, M.; Ilnicka, A.; Lukaszewicz, J.P. The effect of nitrogen species on the catalytic properties of N-doped graphene. *Sci. Rep.* **2021**, *11*, 23970. [CrossRef]
71. Wang, Z.; Li, P.; Chen, Y.; He, J.; Zhang, W.; Schmidt, O.G.; Li, Y. Pure thiophene-sulfur doped reduced graphene oxide: Synthesis, structure, and electrical properties. *Nanoscale* **2014**, *6*, 7281–7287. [CrossRef]
72. Wang, Q.; Ji, Y.; Lei, Y.; Wang, Y.; Wang, Y.; Li, Y.; Wang, S. Pyridinic-N-dominated doped defective graphene as a superior oxygen electrocatalyst for ultrahigh-energy-density Zn-air batteries. *ACS Energy Lett.* **2018**, *3*, 1183–1191. [CrossRef]
73. Ma, R.; Ren, X.; Xia, B.Y.; Zhou, Y.; Sun, C.; Liu, Q.; Liu, J.; Wang, J. Novel synthesis of N-doped graphene as an efficient electrocatalyst towards oxygen reduction. *Nano Res.* **2016**, *9*, 808–819. [CrossRef]
74. Miao, H.; Li, S.; Wang, Z.; Sun, S.; Kuang, M.; Liu, Z.; Yuan, J. Enhancing the pyridinic N content of Nitrogen-doped graphene and improving its catalytic activity for oxygen reduction reaction. *Int. J. Hydrogen Energy* **2017**, *42*, 28298–28308. [CrossRef]
75. Fernández-Sáez, N.; Villela-Martinez, D.E.; Carrasco-Marín, F.; Pérez-Cadenas, A.F.; Pastrana-Martínez, L.M. Heteroatom-doped graphene aerogels and carbon-magnetite catalysts for the heterogeneous electro-Fenton degradation of acetaminophen in aqueous solution. *J. Catal.* **2019**, *378*, 68–79. [CrossRef]
76. Zhai, C.; Sun, M.; Zhu, M.; Song, S.; Jiang, S. A new method to synthesize sulfur-doped graphene as effective metal-free electrocatalyst for oxygen reduction reaction. *Appl. Surf. Sci.* **2017**, *407*, 503–508. [CrossRef]
77. Wang, M.; Li, Y.; Fang, J.; Villa, C.J.; Xu, Y.; Hao, S.; Li, J.; Liu, Y.; Wolverton, C.; Chen, X. Superior oxygen reduction reaction on phosphorus-doped carbon dot/graphene aerogel for all-solid-state flexible Al-air batteries. *Adv. Energy Mater.* **2020**, *10*, 1902736. [CrossRef]
78. Li, R.; Wei, Z.; Gou, X.; Xu, W. Phosphorus-doped graphene nanosheets as efficient metal-free oxygen reduction electrocatalysts. *RSC Adv.* **2013**, *3*, 9978–9984. [CrossRef]
79. Musico, Y.L.F.; Kakati, N.; Labata, M.F.M.; Ocon, J.D.; Chuang, P.-Y.A. One-pot hydrothermal synthesis of heteroatom co-doped with fluorine on reduced graphene oxide for enhanced ORR activity and stability in alkaline media. *Mater. Chem. Phys.* **2019**, *236*, 121804. [CrossRef]
80. Tam, T.V.; Kang, S.G.; Kim, M.H.; Lee, S.G.; Hur, S.H.; Chung, J.S.; Choi, W.M. Novel graphene hydrogel/B-doped graphene quantum dots composites as trifunctional electrocatalysts for Zn− air batteries and overall water splitting. *Adv. Energy Mater.* **2019**, *9*, 1900945. [CrossRef]
81. Nankya, R.; Lee, J.; Opar, D.O.; Jung, H. Electrochemical behavior of boron-doped mesoporous graphene depending on its boron configuration. *Appl. Surf. Sci.* **2019**, *489*, 552–559. [CrossRef]
82. Kumar, R.; Sahoo, S.; Joanni, E.; Singh, R.K.; Maegawa, K.; Tan, W.K.; Kawamura, G.; Kar, K.K.; Matsuda, A. Heteroatom doped graphene engineering for energy storage and conversion. *Mater. Today* **2020**, *39*, 47–65. [CrossRef]
83. Zheng, Y.; Jiao, Y.; Ge, L.; Jaroniec, M.; Qiao, S.Z. Two-step boron and nitrogen doping in graphene for enhanced synergistic catalysis. *Angew. Chem.* **2013**, *125*, 3192–3198. [CrossRef]
84. Su, Y.; Zhang, Y.; Zhuang, X.; Li, S.; Wu, D.; Zhang, F.; Feng, X. Low-temperature synthesis of nitrogen/sulfur co-doped three-dimensional graphene frameworks as efficient metal-free electrocatalyst for oxygen reduction reaction. *Carbon* **2013**, *62*, 296–301. [CrossRef]
85. Han, C.; Chen, Z. The mechanism study of oxygen reduction reaction (ORR) on non-equivalent P, N co-doped graphene. *Appl. Surf. Sci.* **2020**, *511*, 145382. [CrossRef]
86. Lin, H.; Chu, L.; Wang, X.; Yao, Z.; Liu, F.; Ai, Y.; Zhuang, X.; Han, S. Boron, nitrogen, and phosphorous ternary doped graphene aerogel with hierarchically porous structures as highly efficient electrocatalysts for oxygen reduction reaction. *New J. Chem.* **2016**, *40*, 6022–6029. [CrossRef]
87. Razmjooei, F.; Singh, K.P.; Song, M.Y.; Yu, J.-S. Enhanced electrocatalytic activity due to additional phosphorous doping in nitrogen and sulfur-doped graphene: A comprehensive study. *Carbon* **2014**, *78*, 257–267. [CrossRef]
88. Zhao, G.; Shi, L.; Xu, J.; Yan, X.; Zhao, T. Role of phosphorus in nitrogen, phosphorus dual-doped ordered mesoporous carbon electrocatalyst for oxygen reduction reaction in alkaline media. *Int. J. Hydrogen Energy* **2018**, *43*, 1470–1478. [CrossRef]
89. Wu, Z.-S.; Yang, S.; Sun, Y.; Parvez, K.; Feng, X.; Müllen, K. 3D nitrogen-doped graphene aerogel-supported Fe_3O_4 nanoparticles as efficient electrocatalysts for the oxygen reduction reaction. *J. Am. Chem. Soc.* **2012**, *134*, 9082–9085. [CrossRef]
90. Bai, J.; Zhu, Q.; Lv, Z.; Dong, H.; Yu, J.; Dong, L. Nitrogen-doped graphene as catalysts and catalyst supports for oxygen reduction in both acidic and alkaline solutions. *Int. J. Hydrogen Energy* **2013**, *38*, 1413–1418. [CrossRef]

91. Kim, I.T.; Song, M.J.; Kim, Y.B.; Shin, M.W. Microwave-hydrothermal synthesis of boron/nitrogen co-doped graphene as an efficient metal-free electrocatalyst for oxygen reduction reaction. *Int. J. Hydrogen Energy* **2016**, *41*, 22026–22033. [CrossRef]
92. Kim, I.T.; Shin, M.W. Synthesis of nitrogen-doped graphene via simple microwave-hydrothermal process. *Mater. Lett.* **2013**, *108*, 33–36. [CrossRef]
93. Sun, X.; Lin, L.; Sun, L.; Zhang, J.; Rui, D.; Li, J.; Wang, M.; Tan, C.; Kang, N.; Wei, D. Low-temperature and rapid growth of large single-crystalline graphene with ethane. *Small* **2018**, *14*, 1702916. [CrossRef] [PubMed]
94. Qiu, H.J.; Du, P.; Hu, K.; Gao, J.; Li, H.; Liu, P.; Ina, T.; Ohara, K.; Ito, Y.; Chen, M. Metal and nonmetal codoped 3D nanoporous graphene for efficient bifunctional electrocatalysis and rechargeable Zn-air batteries. *Adv. Mater.* **2019**, *31*, 1900843. [CrossRef]
95. Wu, Z.; Zhang, Y.; Li, L.; Zhao, Y.; Shen, Y.; Wang, S.; Shao, G. Nitrogen-doped vertical graphene nanosheets by high-flux plasma enhanced chemical vapor deposition as efficient oxygen reduction catalysts for Zn-air batteries. *J. Mater. Chem. A* **2020**, *8*, 23248–23256. [CrossRef]
96. Wei, D.; Liu, Y.; Wang, Y.; Zhang, H.; Huang, L.; Yu, G. Synthesis of N-doped graphene by chemical vapor deposition and its electrical properties. *Nano Lett.* **2009**, *9*, 1752–1758. [CrossRef]
97. Yazici, M.S.; Azder, M.A.; Salihoglu, O. CVD grown graphene as catalyst for acid electrolytes. *Int. J. Hydrogen Energy* **2018**, *43*, 10710–10716. [CrossRef]
98. Yang, J.; Hu, P.; Yu, G. Design of carbon sources: Starting point for chemical vapor deposition of graphene. *2D Mater.* **2019**, *6*, 042003. [CrossRef]
99. Shinde, D.B.; Chaturvedi, P.; Vlassiouk, I.V.; Smirnov, S.N. Unique role of dimeric carbon precursors in graphene growth by chemical vapor deposition. *Carbon Trends* **2021**, *5*, 100093. [CrossRef]
100. Granzier-Nakajima, T.; Fujisawa, K.; Anil, V.; Terrones, M.; Yeh, Y.-T. Controlling nitrogen doping in graphene with atomic precision: Synthesis and characterization. *Nanomaterials* **2019**, *9*, 425. [CrossRef]
101. Qu, L.; Liu, Y.; Baek, J.-B.; Dai, L. Nitrogen-doped graphene as efficient metal-free electrocatalyst for oxygen reduction in fuel cells. *ACS Nano* **2010**, *4*, 1321–1326. [CrossRef]
102. Wu, X.; Xie, Z.; Sun, M.; Lei, T.; Zuo, Z.; Xie, X.; Liang, Y.; Huang, Q. Edge-rich and (N,S)-doped 3D porous graphene as an efficient metal-free electrocatalyst for the oxygen reduction reaction. *RSC Adv.* **2016**, *6*, 90384–90387. [CrossRef]
103. Xu, J.; Dong, G.; Jin, C.; Huang, M.; Guan, L. Sulfur and nitrogen co-doped, few-layered graphene oxide as a highly efficient electrocatalyst for the oxygen-reduction reaction. *ChemSusChem* **2013**, *6*, 493–499. [CrossRef] [PubMed]
104. Zhuang, S.; Nunna, B.B.; Mandal, D.; Lee, E.S. A review of nitrogen-doped graphene catalysts for proton exchange membrane fuel cells-synthesis, characterization, and improvement. *Nano-Struct. Nano-Objects* **2018**, *15*, 140–152. [CrossRef]
105. Wang, H.-F.; Tang, C.; Zhang, Q. Template growth of nitrogen-doped mesoporous graphene on metal oxides and its use as a metal-free bifunctional electrocatalyst for oxygen reduction and evolution reactions. *Catal. Today* **2018**, *301*, 25–31. [CrossRef]
106. Shi, J.-L.; Tang, C.; Huang, J.-Q.; Zhu, W.; Zhang, Q. Effective exposure of nitrogen heteroatoms in 3D porous graphene framework for oxygen reduction reaction and lithium-sulfur batteries. *J. Energy Chem.* **2018**, *27*, 167–175. [CrossRef]
107. Sharma, P.; Minakshi Sundaram, M.; Watcharatharapong, T.; Laird, D.; Euchner, H.; Ahuja, R. Zn Metal Atom Doping on the Surface Plane of One-Dimesional NiMoO4 Nanorods with Improved Redox Chemistry. *ACS Appl. Mater. Interfaces* **2020**, *12*, 44815–44829. [CrossRef]
108. Sharma, P.; Minakshi Sundaram, M.; Watcharatharapong, T.; Jungthawan, S.; Ahuja, R. Tuning the Nanoparticle Interfacial Properties and Stability of the Core-Shell Structure in Zn-Doped $NiMoO_4$@AWO_4. *ACS Appl. Mater. Interfaces* **2021**, *13*, 56116–56130. [CrossRef] [PubMed]
109. Ito, Y.; Qiu, H.J.; Fujita, T.; Tanabe, Y.; Tanigaki, K.; Chen, M. Bicontinuous nanoporous N-doped graphene for the oxygen reduction reaction. *Adv. Mater.* **2014**, *26*, 4145–4150. [CrossRef]
110. Neupane, S.; Li, W. Carbon nanotube arrays: Synthesis, properties, and applications. In *Three-Dimensional Nanoarchitectures*; Springer: Berlin/Heidelberg, Germany, 2011; pp. 261–285.
111. Anzar, N.; Hasan, R.; Tyagi, M.; Yadav, N.; Narang, J. Carbon nanotube-A review on Synthesis, Properties and plethora of applications in the field of biomedical science. *Sens. Int.* **2020**, *1*, 100003. [CrossRef]
112. Wu, Z.; Song, M.; Wang, J.; Liu, X. Recent progress in nitrogen-doped metal-free electrocatalysts for oxygen reduction reaction. *Catalysts* **2018**, *8*, 196. [CrossRef]
113. Gong, K.; Du, F.; Xia, Z.; Durstock, M.; Dai, L. Nitrogen-doped carbon nanotube arrays with high electrocatalytic activity for oxygen reduction. *Science* **2009**, *323*, 760–764. [CrossRef]
114. Huang, B.; Peng, L.; Yang, F.; Liu, Y.; Xie, Z. Improving ORR activity of carbon nanotubes by hydrothermal carbon deposition method. *J. Energy Chem.* **2017**, *26*, 712–718. [CrossRef]
115. Sa, Y.J.; Park, C.; Jeong, H.Y.; Park, S.H.; Lee, Z.; Kim, K.T.; Park, G.G.; Joo, S.H. Carbon nanotubes/heteroatom-doped carbon core-sheath nanostructures as highly active, metal-free oxygen reduction electrocatalysts for alkaline fuel cells. *Angew. Chem.* **2014**, *126*, 4186–4190. [CrossRef]
116. He, H.; Pham-Huy, L.A.; Dramou, P.; Xiao, D.; Zuo, P.; Pham-Huy, C. Carbon nanotubes: Applications in pharmacy and medicine. *BioMed Res. Int.* **2013**, *2013*, 578250. [CrossRef]
117. Poudel, Y.R.; Li, W. Synthesis, properties, and applications of carbon nanotubes filled with foreign materials: A review. *Mater. Today Phys.* **2018**, *7*, 7–34. [CrossRef]

118. Trogadas, P.; Fuller, T.F.; Strasser, P. Carbon as catalyst and support for electrochemical energy conversion. *Carbon* **2014**, *75*, 5–42. [CrossRef]
119. Ratso, S.; Kruusenberg, I.; Sarapuu, A.; Rauwel, P.; Saar, R.; Joost, U.; Aruväli, J.; Kanninen, P.; Kallio, T.; Tammeveski, K. Enhanced oxygen reduction reaction activity of iron-containing nitrogen-doped carbon nanotubes for alkaline direct methanol fuel cell application. *J. Power Source* **2016**, *332*, 129–138. [CrossRef]
120. Choi, C.H.; Chung, M.W.; Kwon, H.C.; Chung, J.H.; Woo, S.I. Nitrogen-doped graphene/carbon nanotube self-assembly for efficient oxygen reduction reaction in acid media. *Appl. Catal. B Environ.* **2014**, *144*, 760–766. [CrossRef]
121. Choi, J.-Y.; Higgins, D.; Chen, Z. Highly durable graphene nanosheet supported iron catalyst for oxygen reduction reaction in PEM fuel cells. *J. Electrochem. Soc.* **2011**, *159*, B86. [CrossRef]
122. Choi, C.H.; Park, S.H.; Woo, S.I. Phosphorus-nitrogen dual doped carbon as an effective catalyst for oxygen reduction reaction in acidic media: Effects of the amount of P-doping on the physical and electrochemical properties of carbon. *J. Mater. Chem.* **2012**, *22*, 12107–12115. [CrossRef]
123. Wang, Y.-X.; Rinawati, M.; Huang, W.-H.; Cheng, Y.-S.; Lin, P.-H.; Chen, K.-J.; Chang, L.-Y.; Ho, K.-C.; Su, W.-N.; Yeh, M.-H. Surface-engineered N-doped carbon nanotubes with B-doped graphene quantum dots: Strategies to develop highly-efficient noble metal-free electrocatalyst for online-monitoring dissolved oxygen biosensor. *Carbon* **2022**, *186*, 406–415. [CrossRef]
124. Lu, X.; Yim, W.-L.; Suryanto, B.H.; Zhao, C. Electrocatalytic oxygen evolution at surface-oxidized multiwall carbon nanotubes. *J. Am. Chem. Soc.* **2015**, *137*, 2901–2907. [CrossRef]
125. Ren, M.; Chang, F.; Miao, R.; He, X.; Yang, L.; Wang, X.; Bai, Z. Strained lattice platinum-palladium alloy nanowires for efficient electrocatalysis. *Inorg. Chem. Front.* **2020**, *7*, 1713–1718. [CrossRef]
126. Chang, F.; Bai, Z.; Li, M.; Ren, M.; Liu, T.; Yang, L.; Zhong, C.-J.; Lu, J. Strain-Modulated Platinum-Palladium Nanowires for Oxygen Reduction Reaction. *Nano Lett.* **2020**, *20*, 2416–2422. [CrossRef] [PubMed]
127. Kong, Z.; Zhang, D.; Lu, Y.; Yang, C.; Du, S.; Li, W.; Tao, L.; Wang, S. Advanced Cathode Electrocatalysts for Fuel Cells: Understanding, Construction, and Application of Carbon-Based and Platinum-Based Nanomaterials. *ACS Mater. Lett.* **2021**, *3*, 1610–1634. [CrossRef]
128. Hu, X.; Wu, Y.; Li, H.; Zhang, Z. Adsorption and activation of O_2 on nitrogen-doped carbon nanotubes. *J. Phys. Chem. C* **2010**, *114*, 9603–9607. [CrossRef]
129. Wang, Y.; Song, W.; Li, M.; Wu, Z. Oxygen reduction reaction mechanisms on heteroatom-doped single-walled carbon nanotube catalysts: Insights from a theoretical study. *J. Electrochem. Soc.* **2019**, *166*, F670. [CrossRef]
130. Zhang, P.; Hou, X.; Mi, J.; He, Y.; Lin, L.; Jiang, Q.; Dong, M. From two-dimension to one-dimension: The curvature effect of silicon-doped graphene and carbon nanotubes for oxygen reduction reaction. *Phys. Chem. Chem. Phys.* **2014**, *16*, 17479–17486. [CrossRef] [PubMed]
131. An, H.; Zhang, R.; Li, Z.; Zhou, L.; Shao, M.; Wei, M. Highly efficient metal-free electrocatalysts toward oxygen reduction derived from carbon nanotubes@ polypyrrole core-shell hybrids. *J. Mater. Chem. A* **2016**, *4*, 18008–18014. [CrossRef]
132. Xie, W.; Li, J.; Song, Y.; Li, S.; Li, J.; Shao, M. Hierarchical carbon Microtube@ Nanotube core-shell structure for high-performance oxygen electrocatalysis and Zn-air battery. *Nano-Micro Lett.* **2020**, *12*, 97. [CrossRef]
133. Jiang, W.-J.; Hu, J.-S.; Zhang, X.; Jiang, Y.; Yu, B.-B.; Wei, Z.-D.; Wan, L.-J. In situ nitrogen-doped nanoporous carbon nanocables as an efficient metal-free catalyst for oxygen reduction reaction. *J. Mater. Chem. A* **2014**, *2*, 10154–10160. [CrossRef]
134. Xue, L.; Li, Y.; Liu, X.; Liu, Q.; Shang, J.; Duan, H.; Dai, L.; Shui, J. Zigzag carbon as efficient and stable oxygen reduction electrocatalyst for proton exchange membrane fuel cells. *Nat. Commun.* **2018**, *9*, 3819. [CrossRef] [PubMed]
135. Pei, Y.; Song, H.; Liu, Y.; Cheng, Y.; Li, W.; Chen, Y.; Fan, Y.; Liu, B.; Lu, S. Boron-nitrogen-doped carbon dots on multi-walled carbon nanotubes for efficient electrocatalysis of oxygen reduction reactions. *J. Colloid Interface Sci.* **2021**, *600*, 865–871. [CrossRef] [PubMed]
136. Patil, I.M.; Lokanathan, M.; Ganesan, B.; Swami, A.; Kakade, B. Carbon nanotube/boron nitride nanocomposite as a significant bifunctional electrocatalyst for oxygen reduction and oxygen evolution reactions. *Chem. Eur. J.* **2017**, *23*, 676–683. [CrossRef]
137. Suryanto, B.H.; Chen, S.; Duan, J.; Zhao, C. Hydrothermally driven transformation of oxygen functional groups at multiwall carbon nanotubes for improved electrocatalytic applications. *ACS Appl. Mater. Interfaces* **2016**, *8*, 35513–35522. [CrossRef] [PubMed]
138. Likodimos, V.; Steriotis, T.A.; Papageorgiou, S.K.; Romanos, G.E.; Marques, R.R.; Rocha, R.P.; Faria, J.L.; Pereira, M.F.; Figueiredo, J.L.; Silva, A.M. Controlled surface functionalization of multiwall carbon nanotubes by HNO_3 hydrothermal oxidation. *Carbon* **2014**, *69*, 311–326. [CrossRef]
139. Huang, Y.; Liao, W. Hierarchical carbon material of N-doped carbon quantum dots in-situ formed on N-doped carbon nanotube for efficient oxygen reduction. *Appl. Surf. Sci.* **2019**, *495*, 143597. [CrossRef]
140. Chen, L.; Cui, X.; Wang, Y.; Wang, M.; Cui, F.; Wei, C.; Huang, W.; Hua, Z.; Zhang, L.; Shi, J. One-Step Hydrothermal Synthesis of Nitrogen-Doped Carbon Nanotubes as an Efficient Electrocatalyst for Oxygen Reduction Reactions. *Chem. Asian J.* **2014**, *9*, 2915–2920. [CrossRef]
141. El-Sawy, A.M.; Mosa, I.M.; Su, D.; Guild, C.J.; Khalid, S.; Joesten, R.; Rusling, J.F.; Suib, S.L. Controlling the active sites of sulfur-doped carbon nanotube-graphene nanolobes for highly efficient oxygen evolution and reduction catalysis. *Adv. Energy Mater.* **2016**, *6*, 1501966. [CrossRef]

142. Alexeyeva, N.; Shulga, E.; Kisand, V.; Kink, I.; Tammeveski, K. Electroreduction of oxygen on nitrogen-doped carbon nanotube modified glassy carbon electrodes in acid and alkaline solutions. *J. Electroanal. Chem.* **2010**, *648*, 169–175. [CrossRef]
143. Alexeyeva, N.; Tammeveski, K.; Lopez-Cudero, A.; Solla-Gullón, J.; Feliu, J. Electroreduction of oxygen on Pt nanoparticle/carbon nanotube nanocomposites in acid and alkaline solutions. *Electrochim. Acta* **2010**, *55*, 794–803. [CrossRef]
144. Wong, W.; Daud, W.; Mohamad, A.; Kadhum, A.; Loh, K.; Majlan, E. Influence of nitrogen doping on carbon nanotubes towards the structure, composition and oxygen reduction reaction. *Int. J. Hydrogen Energy* **2013**, *38*, 9421–9430. [CrossRef]
145. Gonzalez, I.Z.; Valenzuela-Muñiz, A.; Alonso-Nuñez, G.; Farías, M.; Gomez, Y.V. Influence of the synthesis parameters in carbon nanotubes doped with nitrogen for oxygen electroreduction. *ECS J. Solid State Sci. Technol.* **2017**, *6*, M3135. [CrossRef]
146. Alexander, C.T.; Abakumov, A.M.; Forslund, R.P.; Johnston, K.P.; Stevenson, K.J. Role of the carbon support on the oxygen reduction and evolution activities in $LaNiO_3$ composite electrodes in alkaline solution. *ACS Appl. Energy Mater.* **2018**, *1*, 1549–1558. [CrossRef]
147. Yang, G.; Choi, W.; Pu, X.; Yu, C. Scalable synthesis of bi-functional high-performance carbon nanotube sponge catalysts and electrodes with optimum C-N-Fe coordination for oxygen reduction reaction. *Energy Environ. Sci.* **2015**, *8*, 1799–1807. [CrossRef]
148. Yasuda, S.; Furuya, A.; Uchibori, Y.; Kim, J.; Murakoshi, K. Iron-nitrogen-doped vertically aligned carbon nanotube electrocatalyst for the oxygen reduction reaction. *Adv. Funct. Mater.* **2016**, *26*, 738–744. [CrossRef]
149. Mi, J.-L.; Liang, J.-H.; Yang, L.-P.; Wu, B.; Liu, L. Effect of Zn on size control and oxygen reduction reaction activity of Co nanoparticles supported on N-doped carbon nanotubes. *Chem. Mater.* **2019**, *31*, 8864–8874. [CrossRef]
150. Yang, L.; Jiang, S.; Zhao, Y.; Zhu, L.; Chen, S.; Wang, X.; Wu, Q.; Ma, J.; Ma, Y.; Hu, Z. Boron-doped carbon nanotubes as metal-free electrocatalysts for the oxygen reduction reaction. *Angew. Chem. Int. Ed.* **2011**, *50*, 7132–7135. [CrossRef]
151. Zhao, Y.; Yang, L.; Chen, S.; Wang, X.; Ma, Y.; Wu, Q.; Jiang, Y.; Qian, W.; Hu, Z. Can boron and nitrogen co-doping improve oxygen reduction reaction activity of carbon nanotubes? *J. Am. Chem. Soc.* **2013**, *135*, 1201–1204. [CrossRef]
152. Zhang, Z.; Yang, S.; Li, H.; Zan, Y.; Li, X.; Zhu, Y.; Dou, M.; Wang, F. Sustainable carbonaceous materials derived from biomass as metal-free electrocatalysts. *Adv. Mater.* **2019**, *31*, 1805718. [CrossRef]
153. Song, M.Y.; Park, H.Y.; Yang, D.S.; Bhattacharjya, D.; Yu, J.S. Seaweed-derived heteroatom-doped highly porous carbon as an electrocatalyst for the oxygen reduction reaction. *ChemSusChem* **2014**, *7*, 1755–1763. [CrossRef]
154. Liu, F.; Liu, L.; Li, X.; Zeng, J.; Du, L.; Liao, S. Nitrogen self-doped carbon nanoparticles derived from spiral seaweeds for oxygen reduction reaction. *RSC Adv.* **2016**, *6*, 27535–27541. [CrossRef]
155. Escobar, B.; Pérez-Salcedo, K.; Alonso-Lemus, I.; Pacheco, D.; Barbosa, R. N-doped porous carbon from *Sargassum* spp. as metal-free electrocatalysts for oxygen reduction reaction in alkaline media. *Int. J. Hydrogen Energy* **2017**, *42*, 30274–30283. [CrossRef]
156. Zhang, X.; Liu, R.; Zang, Y.; Liu, G.; Wang, G.; Zhang, Y.; Zhang, H.; Zhao, H. Co/CoO nanoparticles immobilized on Co-N-doped carbon as trifunctional electrocatalysts for oxygen reduction, oxygen evolution and hydrogen evolution reactions. *Chem. Commun.* **2016**, *52*, 5946–5949. [CrossRef] [PubMed]
157. Liu, R.; Zhang, H.; Liu, S.; Zhang, X.; Wu, T.; Ge, X.; Zang, Y.; Zhao, H.; Wang, G. Shrimp-shell derived carbon nanodots as carbon and nitrogen sources to fabricate three-dimensional N-doped porous carbon electrocatalysts for the oxygen reduction reaction. *Phys. Chem. Chem. Phys.* **2016**, *18*, 4095–4101. [CrossRef] [PubMed]
158. Wang, H.; Wang, K.; Song, H.; Li, H.; Ji, S.; Wang, Z.; Li, S.; Wang, R. N-doped porous carbon material made from fish-bones and its highly electrocatalytic performance in the oxygen reduction reaction. *RSC Adv.* **2015**, *5*, 48965–48970. [CrossRef]
159. Liu, F.; Peng, H.; You, C.; Fu, Z.; Huang, P.; Song, H.; Liao, S. High-performance doped carbon catalyst derived from nori biomass with melamine promoter. *Electrochim. Acta* **2014**, *138*, 353–359. [CrossRef]
160. Ilnicka, A.; Skorupska, M.; Tyc, M.; Kowalska, K.; Kamedulski, P.; Zielinski, W.; Lukaszewicz, J.P. Green algae and gelatine derived nitrogen rich carbon as an outstanding competitor to Pt loaded carbon catalysts. *Sci. Rep.* **2021**, *11*, 7084. [CrossRef]
161. Xuan, C.; Wu, Z.; Lei, W.; Wang, J.; Guo, J.; Wang, D. Nitrogen-Doped Hierarchical Porous Carbons Derived from Sodium Alginate as Efficient Oxygen Reduction Reaction Electrocatalysts. *ChemCatChem* **2017**, *9*, 809–815. [CrossRef]
162. Shu, J.; Niu, Q.; Wang, N.; Nie, J.; Ma, G. Alginate derived Co/N doped hierarchical porous carbon microspheres for efficient oxygen reduction reaction. *Appl. Surf. Sci.* **2019**, *485*, 520–528. [CrossRef]
163. Ilnicka, A.; Lukaszewicz, J.P.; Shimanoe, K.; Yuasa, M. Urea treatment of nitrogen-doped carbon leads to enhanced performance for the oxygen reduction reaction. *J. Mater. Res.* **2018**, *33*, 1612–1624. [CrossRef]
164. Guo, D.; Wei, H.; Chen, X.; Liu, M.; Ding, F.; Yang, Z.; Yang, Y.; Wang, S.; Yang, K.; Huang, S. 3D hierarchical nitrogen-doped carbon nanoflower derived from chitosan for efficient electrocatalytic oxygen reduction and high performance lithium-sulfur batteries. *J. Mater. Chem. A* **2017**, *5*, 18193–18206. [CrossRef]
165. Rybarczyk, M.K.; Gontarek, E.; Lieder, M.; Titirici, M.-M. Salt melt synthesis of curved nitrogen-doped carbon nanostructures: ORR kinetics boost. *Appl. Surf. Sci.* **2018**, *435*, 543–551. [CrossRef]
166. El-Nagar, G.A.; Hassan, M.A.; Fetyan, A.; Kayarkatte, M.K.; Lauermann, I.; Roth, C. A promising N-doped carbon-metal oxide hybrid electrocatalyst derived from crustacean's shells: Oxygen reduction and oxygen evolution. *Appl. Catal. B Environ.* **2017**, *214*, 137–147. [CrossRef]
167. Rybarczyk, M.K.; Lieder, M.; Jablonska, M. N-doped mesoporous carbon nanosheets obtained by pyrolysis of a chitosan-melamine mixture for the oxygen reduction reaction in alkaline media. *RSC Adv.* **2015**, *5*, 44969–44977. [CrossRef]

168. Wu, K.H.; Wang, D.W.; Su, D.S.; Gentle, I.R. A discussion on the activity origin in metal-free nitrogen-doped carbons for oxygen reduction reaction and their mechanisms. *ChemSusChem* **2015**, *8*, 2772–2788. [CrossRef]
169. Chen, X.; Liang, Y.; Wan, L.; Xie, Z.; Easton, C.D.; Bourgeois, L.; Wang, Z.; Bao, Q.; Zhu, Y.; Tao, S. Construction of porous N-doped graphene layer for efficient oxygen reduction reaction. *Chem. Eng. Sci.* **2019**, *194*, 36–44. [CrossRef]
170. Tan, A.-D.; Wang, Y.-F.; Fu, Z.-Y.; Tsiakaras, P.; Liang, Z.-X. Highly effective oxygen reduction reaction electrocatalysis: Nitrogen-doped hierarchically mesoporous carbon derived from interpenetrated nonporous metal-organic frameworks. *Appl. Catal. B Environ.* **2017**, *218*, 260–266. [CrossRef]
171. Yang, H.; Kou, S.; Li, Z.; Chang, Z.; Wang, M.; Liu, Z.; Lu, G. 3D interconnected nitrogen-self-doped carbon aerogels as efficient oxygen reduction electrocatalysts derived from biomass gelatin. *RSC Adv.* **2019**, *9*, 40301–40308. [CrossRef]
172. Nam, G.; Park, J.; Kim, S.T.; Shin, D.-B.; Park, N.; Kim, Y.; Lee, J.-S.; Cho, J. Metal-Free Ketjenblack Incorporated Nitrogen-Doped Carbon Sheets Derived from Gelatin as Oxygen Reduction Catalysts. *Nano Lett.* **2014**, *14*, 1870–1876. [CrossRef]
173. Wang, Z.-L.; Xu, D.; Zhong, H.-X.; Wang, J.; Meng, F.-L.; Zhang, X.-B. Gelatin-derived sustainable carbon-based functional materials for energy conversion and storage with controllability of structure and component. *Sci. Adv.* **2015**, *1*, e1400035. [CrossRef]
174. Schnepp, Z.; Zhang, Y.; Hollamby, M.J.; Pauw, B.R.; Tanaka, M.; Matsushita, Y.; Sakka, Y. Doped-carbon electrocatalysts with trimodal porosity from a homogeneous polypeptide gel. *J. Mater. Chem. A* **2013**, *1*, 13576–13581. [CrossRef]
175. Liu, Z.; Li, Z.; Ma, J.; Dong, X.; Ku, W.; Wang, M.; Sun, H.; Liang, S.; Lu, G. Nitrogen and cobalt-doped porous biocarbon materials derived from corn stover as efficient electrocatalysts for aluminum-air batteries. *Energy* **2018**, *162*, 453–459. [CrossRef]
176. Pan, F.; Cao, Z.; Zhao, Q.; Liang, H.; Zhang, J. Nitrogen-doped porous carbon nanosheets made from biomass as highly active electrocatalyst for oxygen reduction reaction. *J. Power Source* **2014**, *272*, 8–15. [CrossRef]
177. Borghei, M.; Laocharoen, N.; Kibena-Põldsepp, E.; Johansson, L.-S.; Campbell, J.; Kauppinen, E.; Tammeveski, K.; Rojas, O.J. Porous N,P-doped carbon from coconut shells with high electrocatalytic activity for oxygen reduction: Alternative to Pt-C for alkaline fuel cells. *Appl. Catal. B Environ.* **2017**, *204*, 394–402. [CrossRef]
178. Liu, Q.; Zhou, Y.; Chen, S.; Wang, Z.; Hou, H.; Zhao, F. Cellulose-derived nitrogen and phosphorus dual-doped carbon as high performance oxygen reduction catalyst in microbial fuel cell. *J. Power Source* **2015**, *273*, 1189–1193. [CrossRef]
179. Wang, J.; Kaskel, S. KOH activation of carbon-based materials for energy storage. *J. Mater. Chem.* **2012**, *22*, 23710–23725. [CrossRef]
180. Lozano-Castelló, D.; Calo, J.M.; Cazorla-Amorós, D.; Linares-Solano, A. Carbon activation with KOH as explored by temperature programmed techniques, and the effects of hydrogen. *Carbon* **2007**, *45*, 2529–2536. [CrossRef]
181. Qiao, W.; Yoon, S.-H.; Mochida, I. KOH Activation of Needle Coke to Develop Activated Carbons for High-Performance EDLC. *Energy Fuels* **2006**, *20*, 1680–1684. [CrossRef]
182. Wang, H.; Gao, Q.; Hu, J. High Hydrogen Storage Capacity of Porous Carbons Prepared by Using Activated Carbon. *J. Am. Chem. Soc.* **2009**, *131*, 7016–7022. [CrossRef]
183. Romanos, J.; Beckner, M.; Rash, T.; Firlej, L.; Kuchta, B.; Yu, P.; Suppes, G.; Wexler, C.; Pfeifer, P. Nanospace engineering of KOH activated carbon. *Nanotechnology* **2011**, *23*, 015401. [CrossRef]
184. Nowicki, P.; Pietrzak, R. Węgle aktywne wzbogacone w azot-otrzymywanie, właściwości i potencjalne zastosowania. *Adsorbenty I Katal.* **2012**, *7*, 129–144.
185. Zhang, J.; Qu, L.; Shi, G.; Liu, J.; Chen, J.; Dai, L. N,P-codoped carbon networks as efficient metal-free bifunctional catalysts for oxygen reduction and hydrogen evolution reactions. *Angew. Chem.* **2016**, *128*, 2270–2274. [CrossRef]
186. Ilnicka, A.; Kamedulski, P.; Skorupska, M.; Lukaszewicz, J.P. Metal-free nitrogen-rich carbon foam derived from amino acids for the oxygen reduction reaction. *J. Mater. Sci.* **2019**, *54*, 14859–14871. [CrossRef]
187. Lin, H.; Chen, D.; Lu, C.; Zhang, C.; Qiu, F.; Han, S.; Zhuang, X. Rational synthesis of N/S-doped porous carbons as high efficient electrocatalysts for oxygen reduction reaction and Zn-Air batteries. *Electrochim. Acta* **2018**, *266*, 17–26. [CrossRef]
188. Kaur, P.; Kim, D.-E.; Verma, G.; Park, J.-S.; Sekhon, S.S. Facile and scalable functionalization of carbon nanofibers for oxygen reduction reaction: Role of nitrogen precursor and non-ionic dispersant. *J. Ind. Eng. Chem.* **2021**, *96*, 307–314. [CrossRef]
189. Massaglia, G.; Margaria, V.; Sacco, A.; Castellino, M.; Chiodoni, A.; Pirri, F.C.; Quaglio, M. N-doped carbon nanofibers as catalyst layer at cathode in single chamber Microbial Fuel Cells. *Int. J. Hydrogen Energy* **2019**, *44*, 4442–4449. [CrossRef]
190. Huang, R.; Cao, C.; Liu, J.; Sun, D.; Song, W. N-Doped carbon nanofibers derived from bacterial cellulose as an excellent metal-free catalyst for selective oxidation of arylalkanes. *Chem. Commun.* **2019**, *55*, 1935–1938. [CrossRef]
191. Boskovic, B.O.; Stolojan, V.; Khan, R.U.; Haq, S.; Silva, S.R.P. Large-area synthesis of carbon nanofibres at room temperature. *Nat. Mater.* **2002**, *1*, 165–168. [CrossRef]
192. Buan, M.E.; Cognigni, A.; Walmsley, J.C.; Muthuswamy, N.; Rønning, M. Active sites for the oxygen reduction reaction in nitrogen-doped carbon nanofibers. *Catal. Today* **2020**, *357*, 248–258. [CrossRef]
193. Minea, T.; Point, S.; Granier, A.; Touzeau, M. Room temperature synthesis of carbon nanofibers containing nitrogen by plasma-enhanced chemical vapor deposition. *Appl. Phys. Lett.* **2004**, *85*, 1244–1246. [CrossRef]
194. Hofmann, S.; Ducati, C.; Robertson, J.; Kleinsorge, B. Low-temperature growth of carbon nanotubes by plasma-enhanced chemical vapor deposition. *Appl. Phys. Lett.* **2003**, *83*, 135–137. [CrossRef]
195. Kong, Y.; Li, Y.; Yang, B.; Li, Z.; Yao, Y.; Lu, J.; Lei, L.; Wen, Z.; Shao, M.; Hou, Y. Boron and nitrogen co-doped porous carbon nanofibers as metal-free electrocatalysts for highly efficient ammonia electrosynthesis. *J. Mater. Chem. A* **2019**, *7*, 26272–26278. [CrossRef]

196. Wu, Q.; Gao, M.; Cao, S.; Hu, J.; Huang, L.; Yu, S.; Ragauskas, A.J. Chitosan-based layered carbon materials prepared via ionic-liquid-assisted hydrothermal carbonization and their performance study. *J. Taiwan Inst. Chem. Eng.* **2019**, *101*, 231–243. [CrossRef]
197. Tong, X.; Chen, Z.; Zhuo, H.; Hu, Y.; Jing, S.; Liu, J.; Zhong, L. Tailoring the physicochemical properties of chitosan-derived N-doped carbon by controlling hydrothermal carbonization time for high-performance supercapacitor application. *Carbohydr. Polym.* **2019**, *207*, 764–774. [CrossRef]
198. Zhu, L.; Shen, F.; Smith, R.L., Jr.; Qi, X. High-Performance Supercapacitor Electrode Materials from Chitosan via Hydrothermal Carbonization and Potassium Hydroxide Activation. *Energy Technol.* **2017**, *5*, 452–460. [CrossRef]
199. Simsir, H.; Eltugral, N.; Karagoz, S. Hydrothermal carbonization for the preparation of hydrochars from glucose, cellulose, chitin, chitosan and wood chips via low-temperature and their characterization. *Bioresour. Technol.* **2017**, *246*, 82–87. [CrossRef]
200. Xu, Z.; Chen, J.; Zhang, X.; Song, Q.; Wu, J.; Ding, L.; Zhang, C.; Zhu, H.; Cui, H. Template-free preparation of nitrogen-doped activated carbon with porous architecture for high-performance supercapacitors. *Microporous Mesoporous Mater.* **2019**, *276*, 280–291. [CrossRef]
201. Shi, J.; Yan, N.; Cui, H.; Liu, Y.; Weng, Y.; Li, D.; Ji, X. Nitrogen doped hierarchically porous carbon derived from glucosamine hydrochloride for CO_2 adsorption. *J. CO2 Util.* **2017**, *21*, 444–449. [CrossRef]
202. Qu, H.; Zhang, X.; Zhan, J.; Sun, W.; Si, Z.; Chen, H. Biomass-Based Nitrogen-Doped Hollow Carbon Nanospheres Derived Directly from Glucose and Glucosamine: Structural Evolution and Supercapacitor Properties. *ACS Sustain. Chem. Eng.* **2018**, *6*, 7380–7389. [CrossRef]
203. Pei, S.; Zhang, J.; Gao, M.; Wu, D.; Yang, Y.; Liu, R. A facile hydrothermal approach towards photoluminescent carbon dots from amino acids. *J. Colloid Interface Sci.* **2015**, *439*, 129–133. [CrossRef]
204. Song, L.-T.; Wu, Z.-Y.; Liang, H.-W.; Zhou, F.; Yu, Z.-Y.; Xu, L.; Pan, Z.; Yu, S.-H. Macroscopic-scale synthesis of nitrogen-doped carbon nanofiber aerogels by template-directed hydrothermal carbonization of nitrogen-containing carbohydrates. *Nano Energy* **2016**, *19*, 117–127. [CrossRef]
205. Gorgieva, S.; Trček, J. Bacterial cellulose: Production, modification and perspectives in biomedical applications. *Nanomaterials* **2019**, *9*, 1352. [CrossRef] [PubMed]
206. Li, R.; Shao, X.; Li, S.; Cheng, P.; Hu, Z.; Yuan, D. Metal-free N-doped carbon nanofibers as an efficient catalyst for oxygen reduction reactions in alkaline and acid media. *Nanotechnology* **2016**, *27*, 505402. [CrossRef] [PubMed]
207. Liang, H.-W.; Wu, Z.-Y.; Chen, L.-F.; Li, C.; Yu, S.-H. Bacterial cellulose derived nitrogen-doped carbon nanofiber aerogel: An efficient metal-free oxygen reduction electrocatalyst for zinc-air battery. *Nano Energy* **2015**, *11*, 366–376. [CrossRef]
208. Park, G.S.; Lee, J.-S.; Kim, S.T.; Park, S.; Cho, J. Porous nitrogen doped carbon fiber with churros morphology derived from electrospun bicomponent polymer as highly efficient electrocatalyst for Zn-air batteries. *J. Power Source* **2013**, *243*, 267–273. [CrossRef]
209. Maldonado, S.; Stevenson, K.J. Influence of Nitrogen Doping on Oxygen Reduction Electrocatalysis at Carbon Nanofiber Electrodes. *J. Phys. Chem. B* **2005**, *109*, 4707–4716. [CrossRef]
210. Yin, J.; Qiu, Y.; Yu, J.; Zhou, X.; Wu, W. Enhancement of electrocatalytic activity for oxygen reduction reaction in alkaline and acid media from electrospun nitrogen-doped carbon nanofibers by surface modification. *RSC Adv.* **2013**, *3*, 15655–15663. [CrossRef]
211. Bokach, D.; ten Hoopen, S.; Muthuswamy, N.; Buan, M.E.; Rønning, M. Nitrogen-doped carbon nanofiber catalyst for ORR in PEM fuel cell stack: Performance, durability and market application aspects. *Int. J. Hydrogen Energy* **2016**, *41*, 17616–17630. [CrossRef]
212. Muthuswamy, N.; Buan, M.E.; Walmsley, J.C.; Rønning, M. Evaluation of ORR active sites in nitrogen-doped carbon nanofibers by KOH post treatment. *Catal. Today* **2018**, *301*, 11–16. [CrossRef]
213. Buan, M.E.; Muthuswamy, N.; Walmsley, J.C.; Chen, D.; Rønning, M. Nitrogen-doped carbon nanofibers on expanded graphite as oxygen reduction electrocatalysts. *Carbon* **2016**, *101*, 191–202. [CrossRef]